PORTLAND PRESS

Research Article

The intracellular domains of the EphB6 and EphA10 receptor tyrosine pseudokinases function as dynamic signalling hubs

Lung-Yu Liang[1,2], Michael Roy[1,2], Christopher R. Horne[1,2], Jarrod J. Sandow[1,2], Minglyanna Surudoi[1], Laura F. Dagley[1,2], Samuel N. Young[1], Toby Dite[1,2], Jeffrey J. Babon[1,2], Peter W. Janes[3], Onisha Patel[1,2], James M. Murphy[1,2] and Isabelle S. Lucet[1,2]

[1]Walter and Eliza Hall Institute or Medical Research, 1G Royal Parade, Parkville, Victoria 3052, Australia; [2]Department of Medical Biology, University of Melbourne, 1G Royal Parade, Parkville, Victoria 3052, Australia; [3]Tumour Targeting Program, Olivia Newton-John Cancer Research Institute and La Trobe School of Cancer Medicine, Level 5, ONJ Centre, 145 Studley Rd, Heidelberg, Victoria 3084, Australia

Correspondence: Onisha Patel (patel.o@wehi.edu.au), James M. Murphy (jamesm@wehi.edu.au) or Isabelle S. Lucet (lucet.i@wehi.edu.au)

OPEN ACCESS

EphB6 and EphA10 are two poorly characterised pseudokinase members of the Eph receptor family, which collectively serves as mediators of contact-dependent cell–cell communication to transmit extracellular cues into intracellular signals. As per their active counterparts, EphB6 and EphA10 deregulation is strongly linked to proliferative diseases. However, unlike active Eph receptors, whose catalytic activities are thought to initiate an intracellular signalling cascade, EphB6 and EphA10 are classified as catalytically dead, raising the question of how non-catalytic functions contribute to Eph receptor signalling homeostasis. In this study, we have characterised the biochemical properties and top-ology of the EphB6 and EphA10 intracellular regions comprising the juxtamembrane (JM) region, pseudokinase and SAM domains. Using small-angle X-ray scattering and cross-linking-mass spectrometry, we observed high flexibility within their intracellular regions in solution and a propensity for interaction between the component domains. We identified tyrosine residues in the JM region of EphB6 as EphB4 substrates, which can bind the SH2 domains of signalling effectors, including Abl, Src and Vav3, consistent with cellular roles in recruiting these proteins for downstream signalling. Furthermore, our finding that EphB6 and EphA10 can bind ATP and ATP-competitive small molecules raises the pros-pect that these pseudokinase domains could be pharmacologically targeted to counter oncogenic signalling.

Introduction

Receptor tyrosine kinases (RTKs) govern all levels of cell proliferation, differentiation and migration [1]. Point mutations and aberrant expression of RTKs that cause hyperactive kinase activity are fre-quently associated with malignancies. Interestingly, 8 out of 58 RTKs contain pseudokinase domains rather than conventional protein kinase domains, and they are predicted to be devoid of catalytic activity [2]. In contrast with conventional protein kinases, pseudokinases are catalytically inactive as they lack one or more key catalytic residues [3–5]. While the biological functions of receptor tyrosine pseudokinases are incompletely understood, changes in their expression level are typically linked to proliferative diseases like cancer. Many pseudokinases exert their non-catalytic functions by allosteri-cally regulating the kinase activity of their kinase-active counterparts [6]. For example, ErbB3/Her3, a pseudokinase of the EGFR family, promotes the tyrosine kinase activity of EGFR via heterodimerisa-tion [7]. Other signalling functions have been proposed for pseudokinases, including nucleating assembly of signalling hubs [8], serving as molecular switches or integrators of signals [9,10], and as competitive signalling effectors [6,11]. Among the receptor tyrosine pseudokinases, PTK7, RYK and

ROR1/2 were recently shown to exhibit conformational plasticity that could be modulated by conventional protein kinase inhibitors [12,13], raising the prospect that they may function as conformational switches. More broadly, understanding the mechanisms by which pseudokinases orchestrate many critical signalling events raises the possibility of novel approaches for therapeutic intervention, including in cancers [14], neurodegenerative [15] and inflammatory diseases [16].

EphB6 and EphA10 are members of the erythropoietin-producing human hepatocellular (Eph) receptors, which comprise the largest RTK protein family. Collectively, Eph receptors govern many developmental processes, such as neuronal development and tissue patterning [17–19], and their expression is often deregulated in cancer [19–21]. This family consists of nine EphA receptors (EphA1–A8 and EphA10) and five EphB receptors (EphB1–B4, EphB6), categorised by sequence similarity and preferential binding to their ephrin-A (ephrin-A1–A5) and ephrin-B (ephrin-B1–B3) ligands [18,21]. Besides their ectodomains, Eph receptors harbour four major intracellular components: an N-terminal juxtamembrane (JM) region, a kinase domain, a sterile α-motif (SAM) domain, and a PDZ domain-binding motif (PBM) located at the C-terminus: a domain architecture shared by EphB6 and EphA10. Upon binding to their membrane-tethered ephrin ligands on an opposing cell through the ectodomains, active Eph receptors undergo dimerisation and oligomerisation [18,21]. The first intracellular event following Eph receptor dimerisation/oligomerisation is autophosphorylation, which in turn creates binding sites on the JM region for downstream Src homology 2 (SH2) domain-containing signalling and adaptor proteins [21]. Eph receptor tyrosine kinase activity, therefore, plays an essential role in signalling; however, the presence of two pseudokinases within the Eph receptor family suggests additional, non-catalytic functions must also contribute to their functions.

The EphB6 and EphA10 pseudokinases are predicted to lack catalytic activity, yet they appear to play crucial roles in signal transduction owing to the association of their deregulated expression with oncogenesis [22–25]. EphB6 expression level is frequently reported to be down-regulated in aggressive malignancies [22,23]. However, recent studies have also reported that EphB6 may accelerate cell proliferation in triple-negative breast cancer cell lines [26], suggesting different mechanisms of action depending on cellular context. Up-regulation of EphA10 expression is also associated with multiple cancers [21,27]. EphB6 was reported to interact with EphA2, EphB1 and EphB4, potentially forming heterodimers and oligomers at the plasma membrane [28–30]. Although the downstream signal transduction upon interacting with kinase-active Eph receptors remains largely unknown, possible EphB6-mediated signalling pathways have been implied from reported interactions with effectors, such as Fyn kinase and Cbl E3 ligase [30,31].

Currently, our functional understanding of the EphB6 pseudokinase is limited, while EphA10 is unstudied. Here, we have undertaken a biochemical and structural characterisation of their intracellular regions to deduce their non-catalytic functions that are critical for signalling. In this study, using small-angle X-ray scattering (SAXS) and cross-linking-mass spectrometry of the intracellular regions of EphB6 and EphA10, we observed high interdomain flexibility in solution, suggesting that the pseudokinase and SAM domains behave largely independently. By mass spectrometry, we identified that the JM region of EphB6 is a substrate of EphB4. Once phosphorylated, the EphB6-JM region provides a binding site for downstream SH2 domain-containing adaptor and signalling proteins, such as Abl, Src and Vav3, which facilitate signal transduction. Like ∼30% of pseudokinases [32], the pseudokinase domains of EphB6 and EphA10 exhibited the propensity to bind ATP, suggesting that a conformational switch might contribute to their regulation, as proposed for other nucleotide-binding pseudokinases [6]. In keeping with this propensity, both EphB6 and EphA10 could bind type I and type II kinase inhibitors, raising the possibility that either may be targetable by small molecule inhibitors.

Materials and methods
DNA construct synthesis and cloning
The DNA constructs encoding human Eph receptors used in this study: EphB6 (residues 625–1021), WT- and FF-ΔN-EphB6 (residues 643–1021), human EphA10 (residues 600–1008), ΔN-EphA10 (residues 618-1008), human WT- and FF-EphB4 (residues 588-987; bearing an N-terminal non-cleavable streptavadin-binding peptide (SBP) tag) were codon optimised for insect cell expression and synthesised by GenScript (Nanjing, China). The resulting constructs were cloned into a vector derived from pFastBac Dual (Invitrogen) under the Polyhedrin promoter that encodes a His$_6$ tag and a TEV protease cleavage sequence N-terminal to the insert. The DNA constructs encoding human SH2 domain inserts: Abl-SH2 (residues 112–232), Vav2-SH2 (residues 667–782), Vav3-SH2 (residues 666–781), Nck1-SH2 (residues 281–377), CrkII-SH2 (residues 6–121),

Grb7-SH2 (residues 415–532), Grb10-SH2 (residues 487–591) were synthesised and subcloned by Genewiz into an in-house modified pCold IV vector (Takara Bio Inc.) bearing a His_8 tag and a TEV protease cleavage sequence. The inserts of human Nck2-SH2 (residues 284–380), CrkL-SH2 (residues 1–104) and Src-SH2 (residues 144–252) domains were obtained by amplifying these sequences from template DNA synthesised by Genewiz. Following subcloning of these inserts into the modified pCold IV vector, insert sequences were validated by Sanger sequencing (Micromon, Monash University, Australia).

Protein expression and purification

EphB6, EphA10 and EphB4 recombinant proteins were expressed in *Spodoptera frugiperda* 21 (*Sf*21) insect cells following infection with baculovirus generated from their pFastBac Dual vectors. Insect cells were cultured at 90 rpm, 27°C for 48 h after baculovirus infection and cells were harvested at $500 \times g$ for 5 min. For protein purification, cell pellets were lysed in 50 ml Lysis Buffer (500 mM NaCl, 10% glycerol, 20 mM Tris, 5 mM imidazole, 0.1% Thesit, 0.5 mM PMSF, 0.5 mM TCEP, pH 8.0) by sonication. The cell lysates were clarified by centrifugation at $38\,500 \times g$ for 30 min, and the supernatant was loaded onto HisTag Ni-NTA resin (Roche). The protein-bound Ni-NTA column was washed intensively using Wash Buffer 1 (500 mM NaCl, 10% glycerol, 20 mM Tris, 10 mM imidazole, 0.1% Thesit, 0.5 mM TCEP, pH 8.0) then Wash Buffer 2 (500 mM NaCl, 10% glycerol, 20 mM Tris, 10 mM imidazole, 0.5 mM TCEP, pH 8.0). Proteins were eluted with Elution Buffer (500 mM NaCl, 10% glycerol, 20 mM Tris, 250 mM imidazole, 0.5 mM TCEP, pH 8.0), followed by concentration and application to a HiLoad 16/600 Superdex 75 column (Cytiva) in SEC Buffer (150 mM NaCl, 5% glycerol, 20 mM Tris, 0.5 mM TCEP, pH 8.0). The protein peak fractions were pooled and TEV protease was added to cleave the N-terminal His_8 tag overnight at 4°C. TEV protease was then eliminated from the preparation by Superdex 200 Increase 10/300 GL (Cytiva) chromatography. The fractions containing the protein of interest were concentrated to 5 mg/ml, aliquoted, snap-frozen and stored in −80°C prior to the subsequent assays.

For SH2 domain constructs, all proteins were expressed in *E. coli* C41(DE3), and purified by Ni-NTA and size exclusion chromatography. Briefly, plasmid-transformed cells were cultured in Super Broth in the presence of 100 µg/ml Ampicillin shaking at 200 rpm, 37°C to OD_{600} 0.6–0.8 before the temperature was reduced to 16°C and expression induced by 0.5 mM IPTG with shaking at 16°C overnight. Cells were pelleted by centrifugation and lysed by sonication in the presence of lysozyme (Sigma) and DNase (Sigma). The purification process was similar to that of Eph recombinant proteins. Protein purity was assessed by analytical SEC with a Superdex 75 Increase 10/300 GL column (Cytiva) and reducing SDS-PAGE with SafeStain visualisation.

Thermal shift assays

A thermal shift assay was used to determine the binding of the nucleotides and kinase inhibitors to EphB6 and EphB4 recombinant proteins; 5–10 µg protein was diluted in Assay Buffer (20 mM HEPES, 150 mM NaCl, pH 7.5) to a total volume of 25 µl in the presence of 250× concentrated SYPRO Orange Stain (Life Technologies, U.S.A.). The concentration of the small molecules tested is indicated in the main text or in the figure legends. Kinase inhibitors were obtained from SYNkinase (Australia). Assays were performed in duplicate in a Rotor-Gene Q PCR machine, using an established method [32–34], where SYPRO Orange was excited at 470 nm, and the emission at 555 nm was recorded. Protein denaturation curves were fitted to the Boltzmann sigmoid equation to obtain the melting temperature (T_m). Independent assays were performed at least twice with consistent results.

Chemical cross-linking experiments

A concentration series of the cross-linkers (Sigma) was used in the presence of 2.5 mg protein in the Assay Buffer. BS^3 (bis(sulfosuccinimidyl)suberate) was used at 2 mM, 1 mM, 0.5 mM, 0.25 mM and 0.1 mM final concentrations; DMTMM (4-(4,6-Dimethoxy-1,3,5-triazin-2-yl)-4-methylmorpholinium chloride) at 100 mM, 60 mM, 30 mM, 15 mM and 7.5 mM. The cross-linking reactions were carried out at 20°C for 30 min and stopped by the addition of reducing SDS-based sample buffer and boiling for 5–10 min. The cross-linked proteins were resolved by SDS–PAGE gel; bands corresponding to the monomeric forms of cross-linked proteins were excised and subjected to in-gel tryptic digest for mass spectrometry identification. Protein bands were visualised with SimplyBlue SafeStain (ThermoFisher) and manually excised for in-gel reduction with 10 mM DTT (Sigma) for 30 min, alkylated for 30 min with 50 mM iodoacetamide (Sigma) and digested with 375 ng Trypsin Gold (Promega) for 16 h at 37°C. The extracted peptide solutions were then acidified (0.1% formic acid) and concentrated to 10 µl by centrifugal lyophilisation using a SpeedVac AES 1010 (Savant). Extracted peptides were injected and separated by reversed-phase liquid chromatography on a M-class UHPLC system

(Waters, U.S.A.) using a 250 mm × 75 μm column (1.6 μm C18, packed emitter tip; IonOpticks, Australia) with a linear 90-min gradient at a flow rate of 400 nl/min from 98% solvent A (0.1% Formic acid in Milli-Q water) to 35% solvent B (0.1% Formic acid, 99.9% acetonitrile). The nano-UPLC was coupled inline to a Q-Exactive Orbitrap mass spectrometer equipped with a nano-electron spray ionisation source (Thermo Fisher Scientific, Bremen, Germany). The Q-Exactive was operated in a data-dependent mode, switching automatically between one full-scan and subsequent MS/MS scans of the ten most abundant peaks. The instrument was controlled using Exactive series version 2.6 and Xcalibur 3.0. Full-scans (m/z 350–1 850) were acquired with a resolution of 70 000 at 200 m/z. The 10 most intense ions were sequentially isolated with a target value of 10 000 ions and an isolation width of 3 m/z and fragmented using HCD with normalised collision energy of 27 and stepped collision energy of 15%. Maximum ion accumulation times were set to 50 ms for full MS scan and 200 ms for MS/MS. Underfill ratio was set to 2% and dynamic exclusion was enabled and set to 30 s.

Raw files were analysed using MaxQuant (version 1.6.5.0). The database search was performed using the Uniprot *Homo sapiens* database plus common contaminants with strict trypsin specificity allowing up to two missed cleavages. MaxQuant APL files were converted to MGF files using the APL to MGF converter software (https://www.wehi.edu.au/people/andrew-webb/1298/apl-mgf-converter). Cross-linked peptides were identified from the MGF files using StavroX software (version 3.6.0.1). Lysines, protein N-termini, serines, threonines and tyrosines were set as reaction sites of the cross-linker NHS-esters (BS[3]) or lysines or protein N-termini linked to aspartic and glutamic acids or protein C-terminus (DMTMM). Trypsin was set as the enzyme allowing for three missed cleavages at lysines and two at arginines. Precursor precision was set at 10 ppm with fragment ion precision set at 20 ppm.

Cross-linked EphB6 peptides were scored based on the mass spectrometry identification confidence. Residues with a cut-off score above 120 were mapped on to a sequence alignment (by Clustal Omega) with EphA2 to identify the equivalent residues. The visualisation was achieved using the PyXlinkViewer [35] Pymol plug-in, where the EphA2 crystal structure (PDB: 7KJB) was used as a model to represent the EphB6 cross-linking events.

Small-angle X-ray scattering experiments

SAXS data were collected at the SAXS/WAXS beamline at the Australian Synchrotron. Protein samples were eluted from an inline Superdex 200 5/150 Increase GL column (Cytiva, Australia) in the path of the X-ray beam [36] via a capillary fitted with a co-flow laminar sheath [37] to eliminate protein exposure to, and fouling of, the capillary wall. 50 μl of 4–5 mg/ml (100–120 μM) protein was injected onto the in-line SEC column pre-equilibrated with SEC Buffer (150 mM NaCl, 5% glycerol, 20 mM Tris, 0.5 mM TCEP, pH 8.0), at 12°C, and the protein was eluted at a flow rate of 0.2 ml/min into the path of the beam where serial 1 s exposures were recorded using an Eiger 2M detector.

The 2D intensity plots corresponding to the protein elution peak were radially averaged, and subtracted by the SEC buffer scattering intensities using the Scatterbrain software package (Stephen Mudie, Australian Synchrotron). The ATSAS software package (Primus) was used to perform Guinier analysis, pairwise distribution function $P(r)$ analysis and to calculate the maximum interparticle dimension (D_{max}) [38]. The molecular mass of proteins was calculated by SAXSMoW [39]. CRYSOL [40] was used to fit the scattering profile to EphA2 crystal structure (PDB: 7KJB and 7KJA) [41] or human EphB6 or EphA10 models derived from AlphaFold [42], and the χ^2 value was used to evaluate the fitting. The data collection and processing statistics are presented in Supplementary Table S1.

In vitro kinase activity assays

Recombinant wild-type EphB6 and SBP-tagged wild-type EphB4 were mixed in equal amounts in the presence of 1 mM ATP and 5 mM MgCl₂. Phosphorylation was allowed to proceed at 20°C for 1 h, and the reaction was stopped by adding reducing SDS sample buffer, boiling for 5–10 min, before proteins were resolved on SDS–PAGE gels and either subjected to Coomassie Blue staining or western blotting using an anti-phosphotyrosine antibody (4G10 clone, Merck, Germany).

Generation of phospho-EphB6 recombinant proteins for surface plasmon resonance

Phosphorylated wild-type EphB6 recombinant proteins were prepared using *in vitro* kinase reactions, as described above. The protein mixture was diluted in Buffer A (20 mM Tris, 5% glycerol, 0.5 mM TCEP, pH 8.0) to a final concentration of 40 mM NaCl, prior to application to MonoQ column (Cytiva) pre-equilibrated

in 4% Buffer B (20 mM Tris, 5% glycerol, 1 M NaCl, 0.5 mM TCEP, pH 8.0). Gradient elution was set as 1% Buffer B/min. The peak fractions corresponding to the non-phosphorylated, P_L and P_H wild-type EphB6 were further purified using a S75 10/300 column in a HEPES-based buffer (20 mM HEPES, 150 mM NaCl, 0.5 mM TCEP, pH 7.5) for optimal protein purity and elimination of Tris buffer prior to biotinylation for the surface plasmon resonance (SPR) experiments.

Identification of phosphorylation sites by mass spectrometry

Protein material was subjected to tryptic digestion using the FASP method as previously described [43,44]. Peptides were lyophilised using CentriVap (Labconco) prior to reconstituting in 25 µl 0.1% FA/2% acetonitrile (ACN). Peptide mixtures (1 µl) were separated by reverse-phase chromatography on a C18-fused silica column (I.D. 75 µm, O.D. 360 µm × 25 cm length) packed into an emitter tip (IonOpticks), using a nano-flow HPLC (Dionex Ultimate 3000). The HPLC was coupled to an Orbitrap Eclipse™ Tribrid (Thermo Scientific) mass spectrometer. Peptides were loaded directly onto the column at a constant flow rate of 400 nl/min with 0.1% formic acid in MilliQ water and eluted with an 18 min linear gradient from 2% to 34% buffer B (99.9% aceto-nitrile and 0.1% formic acid). MS1 spectra were acquired in the Orbitrap ($R = 60$ k; normalised AGC target = 200%; MaxIT = Auto; RF Lens = 30%; scan range = 350–1500; profile data). Dynamic exclusion was employed for 30 s excluding all charge states for a given precursor. MS2 spectra were collected in the Orbitrap ($R = 15$ k; first mass = 120 m/z; normalised AGC target = 200%; MaxIT = 45 ms).

Raw files consisting of high-resolution MS/MS spectra were processed with MaxQuant (version 1.6.17.0) for feature detection and protein identification using the Andromeda search engine as previously described [45]. Extracted peak lists were searched against the reviewed *H. sapiens* (UniProt, August 2020) database as well as a separate reverse decoy database to empirically assess the false discovery rate (FDR) using strict trypsin specificity, allowing up to two missed cleavages. The mass tolerance for precursor ions and fragment ions were 20 ppm and 0.5 Da, respectively. The search included fixed modification of carbamidomethyl (cysteine) and variable modifications including oxidation (methionine), phosphorylation (serine, threonine or tyrosine) and Protein-N terminal acetylation. PSM and protein identifications were filtered using a target-decoy approach at an FDR of 1%. MS spectra were manually validated using IPSA (http://www.interactivepeptidespectralannotator.com) [46].

Surface plasmon resonance experiments

To measure interactions of (pY)-EphB6 with SH2 domains, non-phosphorylated and pTyr EphB6 recombinant proteins in HEPES-based buffer were pre-biotinylated using EZ-Link™ NHS-PEG$_4$-Biotin (A39259, ThermoFisher Scientific, Australia) according to the manufacturer's instructions, and immobilised on Series S streptavidin (SA) sensor chips (GE Healthcare Life Sciences, Sweden), with immobilisation levels indicated in the figure legends. SPR experiments with SH2 domains were carried out with the following parameters (flow rate 10 µl/min, injection contact time 120 sec, dissociation time 340–440 sec). A regeneration step using 1 M NaCl was included after each binding cycle (regeneration cycle injection time 30 sec, flow rate 30 µl/min) to ensure the response units of each cycle return to the baseline.

To measure interactions between (pY)-EphB6 peptides and SH2 domains, SH2 domains were immobilised by amine coupling onto Series S CM5 chips (Cytiva) in either 10 mM acetic acid solution, pH 5.5 or 10 mM HEPES solution, pH 7.0 as the immobilisation buffer depending on the pI of the proteins. EDC, NHS and ethanolamine from the amine coupling kit (Cytiva, US) were used according to the manufacturer's instructions. The final immobilisation level of each protein is indicated in the figure legends. (pY)-EphB6 peptides synthe-sised to >95% purity (Mimotopes, Australia) were reconstituted in 100 mM Tris, pH 8.0 to a final concentra-tion of 5 mM; the pH of all the stock solution was confirmed as approximately pH 7.5 using pH strips. Peptides were diluted in Running Buffer (10 mM HEPES, 150 mM NaCl, 3 mM EDTA, 0.005% Tween 20, 0.5 mM TCEP, pH 7.5) to the concentrations used in the SPR experiments (flow rate 10 µl/min, contact time injection 120 sec, dissociation time 200–600 sec). A regeneration step using 50 mM phenyl phosphate in the Running Buffer was included after each binding cycle (regeneration cycle injection time 30 sec, flow rate 30 µl/min) to ensure the response units of each cycle returned to the baseline.

All SPR binding experiments were run on a Biacore S200 instrument with Running Buffer. The sample holder was set at 12°C and binding measurements were performed at 20°C. The dissociation constant, K_D, was calculated by fitting the experimental data to a 1 : 1 steady-state binding affinity model. At least three independ-ent measurements were performed to calculate the K_D.

Results

The pseudokinase domains of EphB6 and EphA10 lack conserved catalytic residues

Protein kinases consist of an N-lobe and C-lobe with an intervening cleft that houses crucial residues that catalyse the transfer of the γ-phosphate from ATP to a protein substrate (Figure 1A). In the N-lobe, the glycine-rich loop plays an important role in ATP binding; and a conserved Lys on the β3-strand plays an essential role in positioning ATP via interaction with the β-phosphate of ATP, as well as maintaining an active kinase conformation through a salt bridge with a conserved Glu in the αC helix. In the C-lobe, the Asp of the HRD motif in the catalytic loop plays an essential role in the transfer of the ATP γ-phosphate to the substrate, while the Asp of the DFG motif binds a Mg^{2+} cofactor, which favourably positions ATP for phosphoryl-transfer. The loss of one or more of these critical residues typically results in the loss of kinase activity, as would be expected for EphB6 and EphA10, which have substitutions of the β3 Lys, and Asp residues in both the activation and catalytic loops (Figure 1B).

In Eph receptors that exhibit catalytic activity, phosphorylation of the conserved JX1 and JX2 tyrosine residues relieves association of the JM region (Figure 1B) with the kinase domain to allow activation of the kinase domain [47,48]. Intriguingly, the JX1 and JX2 tyrosine residues are conserved in EphB6, but not EphA10 (Figure 1B). Thus, it is of interest to deduce the functional role of JX1 and JX2 in EphB6 and, in particular, whether phosphorylation of these residues by their catalytically active Eph receptor cousins might regulate EphB6 function.

EphB6 and EphA10 pseudokinase domains bind nucleotides

Pseudokinases can be broadly categorised into four subgroups, based on their nucleotide-binding properties: (1) non-binding, (2) nucleotide binding, (3) cation binding and (4) nucleotide and cation binding [32]. Given that nucleotide binding propensity has been proposed to reflect the capacity of pseudokinases to adopt multiple conformations, we examined the nucleotide-binding abilities of the intracellular domains of both EphB6 and EphA10 using thermal stability assays. Each of EphB6 and EphA10 bound ATP with an apparent K_D of 94 μM and 95 μM, respectively (Figure 1C,D and Supplementary Figure S1B–E), which is comparable to the affinities of many kinase and pseudokinase domains for ATP [49,50]. Inclusion of the flanking JM region and SAM domains did not impinge upon the capacity of EphB6 to bind ATP, which had previously been reported qualitatively for its core pseudokinase domain [32]. Interestingly, the presence of Mg^{2+} decreased EphB6 and EphA10 protein stability (Supplementary Figure S1B,C). This may be due to substitutions of the Mg^{2+}-binding Asp in the DFG motif at the start of the activation loop of conventional protein kinases, where substitutions of DFG to RLG for EphB6 or GFG for EphA10 could give rise to activation loop disorganisation in the presence of Mg^{2+}. We then assessed whether EphB6 and EphA10 can bind kinase inhibitors with different modes of action. Type I and II kinase inhibitors lock the kinase domains in an active and an inactive conformation, respectively. Remarkably, both EphB6 and EphA10 are able to bind both Type I (Dasatinib) and Type II (AMG Tie2-1) kinase inhibitors. While the binding of both Type I and Type II inhibitors appear to be tighter compared with ATP, we were not able to reliably estimate the K_D values, as the binding seems to be accompanied by a conformational transition (Figure 1E–H and Supplementary Figure S1B,C). These data suggest that EphB6 and EphA10 pseudokinase domains can sample different conformations, which might reflect a molecular switch function that has been proposed for other ATP-binding pseudokinases [9,12,32,50]. Although the biological consequences of EphB6 and EphA10 binding to ATP in cells remains to be investigated, our data suggest that the conformations of their pseudokinase domains can be modulated by ATP and ATP competitive kinase inhibitors.

The intracellular domains of EphB6 and EphA10 exist as monomers

Kinase-competent Eph receptors autophosphorylate upon dimerisation/oligomerisation. While oligomerisation has been proposed to be primarily driven by ligand binding to the extracellular domain and by the oligomerisation properties of the extracellular domain [21,51], the presence of dimerisation/oligomerisation domains within the intracellular region raises the possibility that the cytoplasmic portion of the receptor might contribute to higher order assemblies [52]. For example, the C-terminal SAM domains of the Eph receptors are characterised as dimerisation/oligomerisation domains known to form higher-order structures [53–56]. Kinase and pseudokinase domains also frequently form stable dimers, with diverse modes of interaction evident from
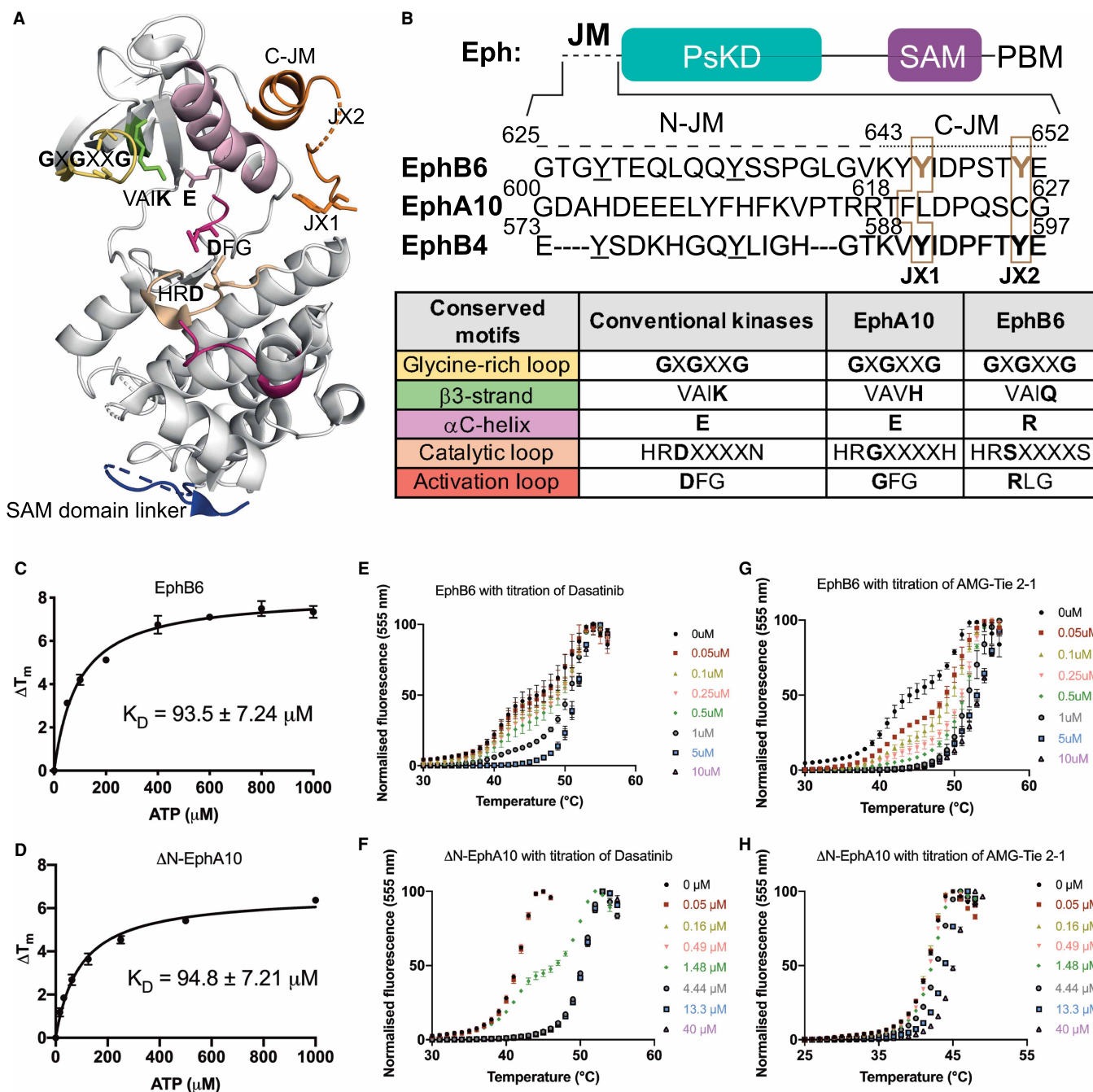
Figure 1. EphB6 and EphA10 pseudokinase domains bind nucleotides and protein kinase inhibitors.

(**A**) An exemplar crystal structure of an Eph receptor kinase domain (EphA3; PDB: 2QO2 [48]), with the conserved motifs (residues) responsible for kinase activity (as tabulated in panel (**B**)) highlighted. (**B**) A schematic diagram showing the intracellular domain/motifs of EphB6/EphA10, which contains the juxtamembrane (JM) region, the pseudokinase domain (PsKD), the sterile-α-motif (SAM) domain and the C-terminal PDZ domain-binding motif (PBM). The sequences of the N-JM and partial C-JM of EphB6, EphA10 and EphB4 are highlighted, with the JX1 and JX2 positions coloured in brown. The underlined tyrosine residues in the N-JM region are conserved in all and only Type B Eph receptors. In the table, the conserved catalytic motifs (residues) required for protein kinase activity, and corresponding residues in the pseudokinase domains of EphB6 and EphA10 are listed. (**C**) The estimated K_D for ATP binding to EphB6 is 94 μM. (**D**) The estimated K_D for ATP binding to ΔN-EphA10 is 95 μM. Titrations of type I (Dasatinib) kinase inhibitor for binding to EphB6 (**E**), ΔN-EphA10 (**F**). Titrations of type II (AMG-Tie 2-1) kinase inhibitors for binding to EphB6 (**G**), ΔN-EphA10 (**H**). Titrations were done in triplicate and error bars represent the standard error of the mean (SEM). At least two independent experiments were carried out for each titration, and representatives are shown here.

structural studies [33,57]. Additionally, most RTKs, including Eph receptors, contain a JM region within the cytoplasmic portion, N-terminal to the kinase domain. In the case of the EGFR receptor family, the JM region is known to play a crucial role in enabling dimerisation of their kinase domains and thus regulation of kinase activation [58,59]. This raises the possibility that the JM regions of EphB6 and EphA10 could function as a latch to augment the formation of higher order pseudokinase domain assemblies.

To examine whether the JM region and SAM domain of EphB6 and EphA10 contribute to higher order assembly, we generated recombinant proteins encompassing all the intracellular domains of EphB6 (residues 625–1021) and EphA10 (residues 600–1008), and versions with the N-terminal portion of the JM region truncated, termed ΔN-EphB6 (residues 643–1021) and ΔN-EphA10 (residues 618–1008) (Figure 1B and Supplementary Figure S1A). By analytical size exclusion chromatography, all four proteins eluted at retention times consistent with them occurring as monomers in solution (Figure 2A). Although we noticed that the EphA10 recombinant protein containing all the intracellular domains eluted markedly earlier in analytical size exclusion chromatography compared with ΔN-EphA10 (Figure 2A), we confirmed its monomeric state by SAXS, where the estimated molecular mass is similar to the predicted monomeric molecular mass (Supplementary Table S1). Furthermore, the radius of gyration (R_g) of EphA10 derived from the inline SEC-SAXS remained constant across the eluted SEC peak, consistent with EphA10 occurring as a monomer in solution (Supplementary Figure S2A). The monomeric states of EphB6 (residues 625–1021), as well as ΔN-EphB6 (residues 643–1021) and N-EphA10 (residues 618–1008), in solution, were also supported by SAXS data (Supplementary Table S1). Together, these data indicate that, under the conditions tested, neither the EphB6 and EphA10 pseudokinase or SAM domains homodimerise and, in contrast with EGFR [59], the N-terminal JM region did not mediate the formation of EphB6 or EphA10 intracellular region higher order assemblies.

The component domains within the EphB6 and EphA10 intracellular regions are not tightly associated in solution

Like other Eph receptors, the pseudokinase and the SAM domains of EphB6 and EphA10 are connected through a ~40 amino acid long SAM domain linker that is predicted to be unstructured. This suggests there is likely to be some conformational plasticity between the pseudokinase and SAM domains, which may allow for intramolecular interaction and potential allosteric regulation. Although yet to be demonstrated, the conformational plasticity of the Eph receptor intracellular domains may decide the propensity of binding to other interactors, such as to the SAM domain-containing effectors [52], which could influence downstream signal transduction.

To obtain insights into the conformations of the EphB6 and EphA10 intracellular regions in solution, and whether ATP binding affects their topology, we performed SAXS experiments. Using an inline size exclusion chromatography setup with elution into the path of the X-ray beam, we subjected the complete intracellular regions of EphB6 and EphA10, and their ΔN JM region counterparts, to SAXS. Guinier analysis indicated that all samples were monodispersed with no evident aggregation or inter-particle interaction (Figure 2B–E and Supplementary Figure S2B–E). In the absence of an EphB6 intracellular domain crystal structure, we compared the experimental scatter of ΔN-EphB6 to the theoretical scatter calculated using the EphB6 structure co-ordinates (EphB6 entry: O15197) generated form AlphaFold [42] using CRYSOL. These co-ordinates showed excellent agreement with the ΔN-EphB6 ($\chi^2 = 0.129$, Figure 2B,F), suggesting the protein conformation in solution resemble closely to that predicted by AlphaFold. As protein structures from AlphaFold are computationally calculated, we sought to also capitalise on experimental crystal structures of the EphA2 intracellular domains, that were recently determined by X-ray crystallography [41]. Our scattering data closely resemble the theoretical scatter calculated for the elongated EphA2 structure (PDB: 7KJB; $\chi^2 = 0.178$, Supplementary Figure S2B). In this conformation, the SAM domain linker is fully extended, moving the SAM domain away from the C-lobe of the kinase domain. A comparison of our scattering data to the theoretical scatter calculated for the more compact EphA2 structure (PDB: 7KJA), however, rendered a poor χ^2 value ($\chi^2 = 1.292$, Supplementary Figure S2J), consistent with ΔN-EphB6 adopting an extended conformation in solution. The presence of AMPPNP (a non-hydrolysable ATP analogue) did not impact the gross topology of ΔN-EphB6, as the scattering profile of AMPPNP-bound ΔN-EphB6 largely resembled its apo form, with a comparable elongated conformation in solution (Figure 2C and Supplementary Figure S2C). Next, we sought to understand if the inclusion of the N-terminal JM region can impact the overall protein conformation in solution. The scatter of the complete intracellular regions of EphB6 and EphA10 compared favourably with the theoretical scatter
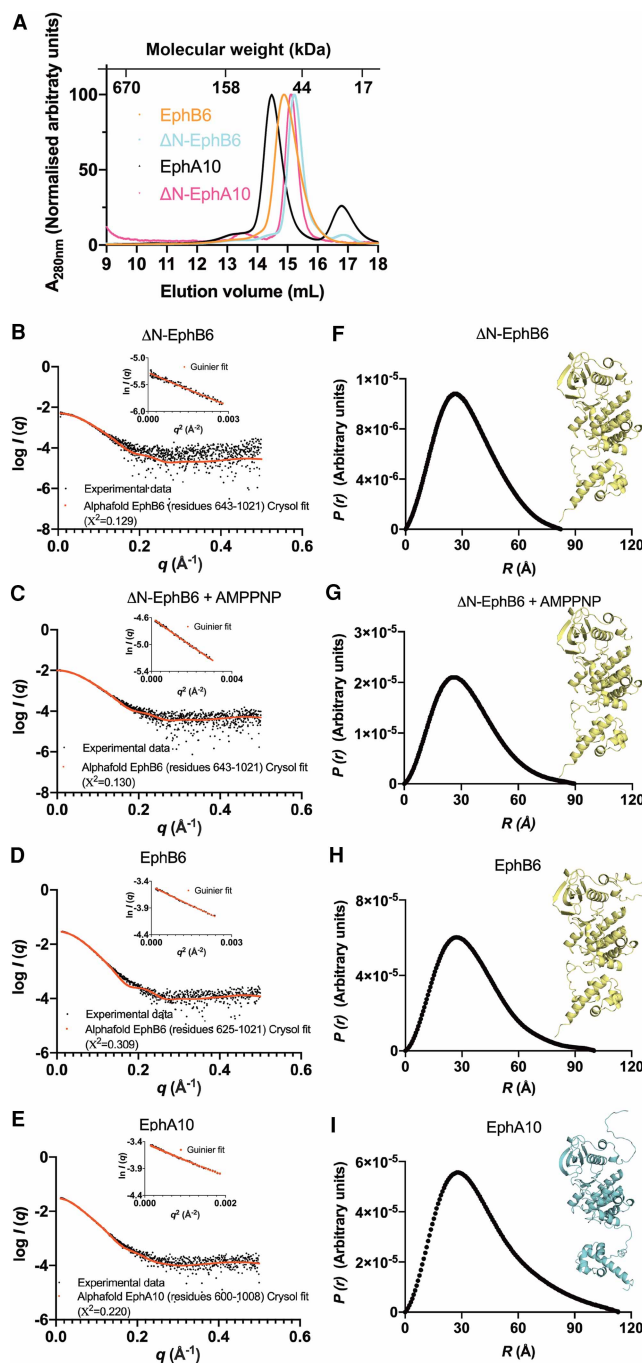
Figure 2. The EphB6 and EphA10 intracellular domains are monomeric and exhibit elongated conformations in solution.

Part 1 of 2

(**A**) Recombinant EphB6 (residues 625–1021), ΔN-EphB6 (residues 643–1021), EphA10 (residues 600–1008) and ΔN-EphA10 (residues 618–1008) elution profiles from an S200 Increase 10/300 GL gel filtration column. The following molecular mass markers, Thyroglobulin (670 kDa), bovine γ-globulin (158 kDa), chicken ovalbumin (44 kDa), equine myoglobin (17 kDa), and vitamin B12 (1.35 kDa) (Bio-Rad) were used to estimate the molecular mass of the eluted proteins. (**B**) The ΔN-EphB6 SAXS profile compared with the theoretical scatter of the AlphaFold EphB6 structure co-ordinates (EphB6 entry: O15197, residues 643–1021) by CRYSOL ($\chi^2 = 0.129$). The Guinier plot (inset) shows monodispersed proteins in solution, free from aggregation and inter-particle interaction. (**C**) The ΔN-EphB6 + AMPPNP SAXS profile compared with the theoretical scatter of the EphB6 structure co-ordinates predicted by AlphaFold (EphB6 entry: O15197, residues 643–1021) by CRYSOL ($\chi^2 = 0.130$). The Guinier plot (inset) shows monodispersed proteins in solution, free from aggregation and inter-particle interaction. (**D**) The EphB6 SAXS

**Figure 2. The EphB6 and EphA10 intracellular domains are monomeric and exhibit elongated conformations
in solution.**
Part 2 of 2

profile fitted to the theoretical scatter of the AlphaFold EphB6 structure co-ordinates (EphB6 entry: O15197, residues
625–1021) by CRYSOL ($\chi^2 = 0.309$). The Guinier plot (inset) shows monodispersed proteins in solution, free from aggregation
and inter-particle interaction. (**E**) The EphA10 SAXS profile fitted to the theoretical scatter of the AlphaFold EphA10 structure
co-ordinates (EphA10 entry: Q5JZY3, residues 600–1008) by CRYSOL ($\chi^2 = 0.220$). The Guinier plot (inset) shows
monodispersed proteins in solution, free from aggregation and inter-particle interaction. Pairwise distribution analysis is shown
for ΔN-EphB6 (**F**), ΔN-EphB6 + AMPPNP (**G**), EphB6 (**H**) and EphA10 (**I**), with the corresponding structures of EphB6 and
EphA10 from AlphaFold presented.

calculated for the relaxed conformation observed in the EphA2 crystal structure (PDB: 7KJB) and the structures
of EphB6 and EphA10 derived from AlphaFold (Figure 2D,E, Supplementary Figure S2D,E), whereas the scat-
tering for each was inconsistent with the EphA2 compact structure (PDB: 7KJA) ($\chi^2 = 9.156$ for EphB6 and χ^2
= 3.495 for EphA10, Supplementary Figure S2J). The inclusion of the JM region in the EphB6 and EphA10
constructs leads to further elongation of the structure, as evident from a larger maximum particle dimension
(D_{max}) in the pairwise distribution analysis (Figure 2F–I), consistent with the N-terminal extension acting
autonomously from the pseudokinase and SAM domains. Dimensionless Kratky plots calculated from the
scatter of each EphB6 and EphA10 construct are consistent with each protein adopting a flexible and asymmet-
ric conformation (Supplementary Figure S2F–I). Such flexibility is reflected in excellent fits of both AlphaFold
models and the elongated experimentally determined EphA2 structure (PDB: 7KJB) to our experimental scat-
tering profiles, and is consistent with the propensity of EphB6 and EphA10 to adopt multiple conformations in
solution.

SAXS allows the calculation of the average shape of a protein of interest, but does not capture transient intra-
and inter-domain interactions. To obtain more detailed information of these transient interactions, we per-
formed chemical cross-linking on the recombinant EphB6 intracellular region using two cross-linkers with dif-
ferent spacer lengths, DMTMM (0 Å) and BS^3 (11.4 Å), resolution by SDS–PAGE, followed by tryptic digest of
the excised monomer gel bands and mass spectrometry to identify the cross-linked peptides. DMTMM cross-
links an amine (N-terminus or Lys sidechain) to the sidechain of an Asp or Glu residues, and as it is a zero-
length cross-linker, it recognises two residues in close proximity that can potentially form salt bridges. BS^3 cross-
links two amine moieties and, owing to an eight-carbon spacer, couples sites 11.4 Å apart. Cross-linked EphB6
resolved by SDS–PAGE remained largely monomeric (Figure 3A), consistent with its behaviour in SEC and
SAXS experiments. We mapped cross-linked amino acids to the EphB6 structure derived from AlphaFold
(Figures 3B,C), and their counterparts on the EphA2 crystal structure (PDB: 7KJB) (Supplementary Figures S3A,
B). In both cases, residues with an estimated 8–15 Å distance within the pseudokinase domain could be cross-
linked by DMTMM (Figure 3B,C, Supplementary Figure S3A,B), suggesting that the EphB6 pseudokinase core is
highly dynamic in solution. Additionally, we identified a cross-linking hotspot on the α5 helix of the SAM
domain, to which residues in both the N-lobe and C-lobe of the pseudokinase domain were zero-length cross-
linked (Figure 3B,C, Supplementary Figure S3A,B). Additionally, the C-terminal PBM cross-linked the αJ helix
of the pseudokinase domain (Figure 3B,C). These data indicate that the SAM domain is highly mobile and can
occupy a vast array of positions around the pseudokinase domain, resulting in high conformational plasticity
within the EphB6 intracellular portion and frequent interdomain interaction. Interestingly, the SAM domain α5
helix interaction hotspot is conserved in all Eph receptors except for EphA10 [21], and contributes to the SAM–
SAM heterodimerisation interface in other receptors, including EphA1, EphA2, EphA5 and EphA6 with their
SAM domain-containing effector proteins [52]. Consequently, we predict that binding of SAM domain-
containing effector proteins downstream of activation of Eph receptors including EphB6 would favour intracellu-
lar region elongation, which may influence the conformation of the Eph kinase/pseudokinase core.

The conserved EphB6 JM domain JX1 and JX2 sites are phosphorylation sites
for EphB4

In contrast with the kinase-active receptors that rely on their catalytic activity for signal transduction, how
EphB6 and EphA10 signal remains unknown. For kinase-active Eph receptors, autophosphorylation of two
conserved tyrosine residues in the C-terminal JM region (named JX1 and JX2, Figure 1B) enables them to
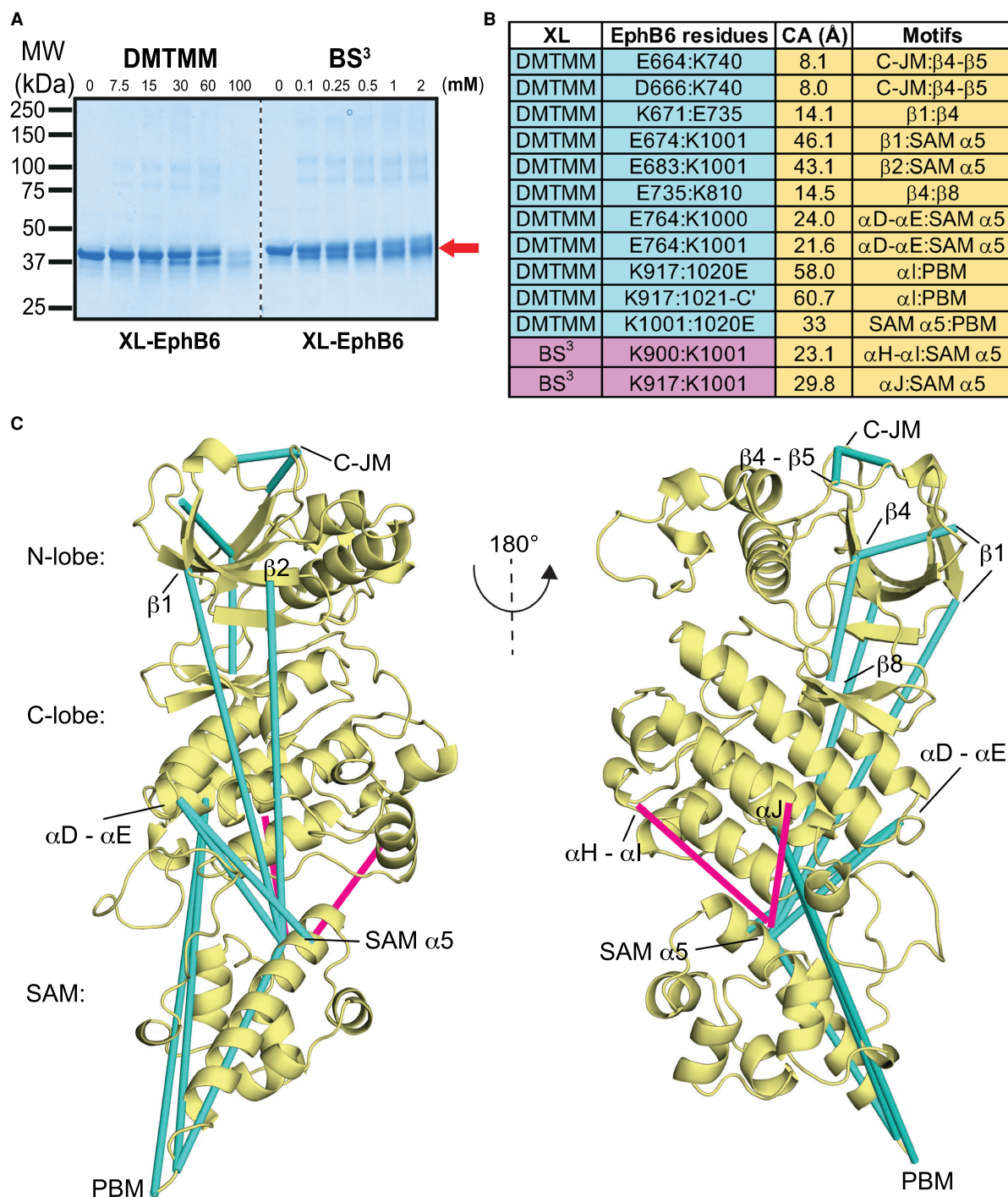
Figure 3. EphB6 intracellular domains exhibit dynamic inter-domain interaction by chemical cross-linking-mass spectrometry experiments.

(**A**) Reducing SDS–PAGE of the EphB6 recombinant proteins cross-linked by a concentration series of DMTMM and BS[3] stained with Simply Blue SafeStain. (**B**) The amino acid residues cross-linked by DMTMM (0 Å spacer) are highlighted in cyan, and the amino acid residues cross-linked by BS[3] (11.4 Å spacer) are highlighted in magenta. The distance of the backbone carbon and the secondary structures in the AlphaFold EphB6 structure (EphB6 entry: O15197, residues 625–1021) are highlighted in light yellow. C′: the carboxylic end of proteins. (**C**) The cross-linked amino acid residues are connected by cyan lines (cross-linked by DMTMM), and by magenta lines (cross-linked by BS[3]) in the Alphafold EphB6 structure (EphB6 entry: O15197, residues 625–1021).

acquire full kinase activity and provides binding sites for SH2 domain-containing proteins. EphB6 harbours the JX1 (Y645) and JX2 (Y651) tyrosines, suggesting EphB6 similarly may engage adaptor proteins via their SH2 domains upon phosphorylation. In EphA10 the equivalent JX1 and JX2 residues are Phe and Cys, respectively, suggesting that for EphA10 engagement of downstream effectors likely relies on distinct mechanisms (Figure 1B). Interestingly, EphB6 contains another conserved tyrosine residue on the α2 helix of the SAM domain (Y965), which, when phosphorylated, has been reported to interact with Grb7 and Grb10 in other Eph receptors such as EphB1 and EphA2 [60,61]. EphB6 also possesses two conserved tyrosine residues located at the N-terminal portion of the JM region that are unique to EphB receptors (Figure 1B), and are thought to underpin distinct regulatory mechanisms in Type A and Type B Eph receptors [21].

We speculated that EphB6 may be regulated via phosphorylation of its tyrosines by kinase-active counterparts to generate binding sites for cytosolic SH2 domain-containing adaptor and effector proteins. EphB1 and EphB4 were previously reported to phosphorylate EphB6 in cells [29,30]; however, the phosphorylation sites were not identified. The lack of molecular detail and the functional consequences resulting from EphB6 phosphorylation prompted us to characterise EphB6 tyrosine phosphorylation sites.

Figure 4. The EphB6 C-terminal JM region is the site of phosphorylation by EphB4.
(**A**) EphB6 recombinant proteins (WT and the YY → FF (JX1 and JX2) mutant) were phosphorylated by recombinant EphB4 (WT and the YY → FF (JX1 and JX2) mutant) *in vitro*. The reaction mixture was resolved by reducing SDS–PAGE and probed using an anti-phosphotyrosine antibody (Clone: 4G10). (**B**) Different phosphorylated EphB6 recombinant proteins: ΔN-EphB6 (P_L: low level of phosphorylation, P_H: high level of phosphorylation) were separated by anion-exchange chromatography (MonoQ column). (**C**) The phosphorylation level of a selected phosphopeptide including pY651 (JX2) and a phosphopeptide including pY669 identified is shown by the relative abundance of phosphorylation in the non-phosphorylated, P_L- and P_H-EphB6 measured by mass spectrometry. (**D**) SEC profiles from an S75 10/300 GL gel filtration column of phosphorylated ΔN-EphB6 recombinant proteins demonstrating that they remain monomeric in solution.

We first generated recombinant EphB4 encompassing the C-terminal portion of the JM region to the PBM (residues 588–987) (Supplementary Figure S1A), which, as expected, was catalytically active (Figure 4A). We then performed *in vitro* kinase activity assays using purified EphB4 as the kinase and EphB6 as its substrate. No basal phosphorylation was detected by western blot and mass spectrometry for the complete EphB6 intracellular region or the ΔN-EphB6 recombinant proteins alone (Figure 4A, Supplementary Figure S4A,B), and neither exhibited any residual catalytic activity, with no autophosphorylation observed upon addition of ATP/Mg^{2+} (Figures 4A, Supplementary Figure S4A,B). In contrast, recombinant EphB4 readily phosphorylated both EphB6 (residues 625–1021) and ΔN-EphB6 (residues 643–1021) (Figure 3A). On the other hand, the Y645F/Y651F ΔN-EphB6 protein (termed FF-ΔN-EphB6) in which the JX1 and JX2 sites were mutated proved to be a much poorer substrate for EphB4 than wild-type EphB6 (Figure 4A, Supplementary Figure S4A,B), implicating the JX1 and JX2 tyrosines as the major phosphorylation sites. In addition, to evaluate whether phosphorylation of the JX1 and JX2 tyrosines is crucial to EphB4 kinase activity, we generated the EphB4 JX1 (Y590) and JX2 (Y596) double phenylalanine mutant (Y590F/Y596F; termed FF-EphB4). By using EphB6 as a substrate, we found that FF-EphB4 retained catalytic activity (Figure 4A), but its kinase activity was reduced relative to the wild-type counterpart, indicating that phosphorylation of the JX1 and JX2 tyrosines is necessary for the kinase to adopt a fully active conformation (Supplementary Figures S4A,B). This is in agreement with previously reported biochemical and structural studies conducted on other Eph receptors [47,48,62,63].

To confirm the precise phosphorylation sites on EphB4-treated EphB6 and ΔN-EphB6 we used mass spectrometry. To our surprise, we did not detect any phosphorylation on the two tyrosine residues (Y628 and Y635) on the N-JM, suggesting these conserved tyrosines in the Type B Eph receptors are not substrates of EphB4. While we were able to identify JX2 (Y651) with high confidence, we were unable to determine unambiguously which of Y644 and the JX1 tyrosine, Y645, were phosphorylated (Supplementary Figure S4C). Although phosphorylation on Y644 was not detected in FF-ΔN-EphB6 (Supplementary Figure S4C), phosphorylation of Y644 may require prior phosphorylation of the adjacent Y645, via a priming mechanism akin to that reported for the EGFR receptor JM region [64]. To explore this possibility, we used anion exchange chromatography to resolve different phosphorylated forms of WT-ΔN-EphB6 for mass spectrometry analysis (Figure 4B). From the phosphorylated elution fractions P$_L$ (low-degree phosphorylated) and P$_H$ (high-degree phosphorylated), we were able to unambiguously identify Y644, Y645 (JX1), Y651 (JX2) and Y669 as the EphB6 sites phosphorylated by EphB4, all of which are located on the C-terminal portion of the JM region (Figure 4C, Supplementary Figure S4D–F). Notably, phosphorylation of ΔN-EphB6 did not influence its oligomeric status; both the highly (P$_H$) and lowly (P$_L$) phosphorylated fractions of ΔN-EphB6 behaved comparably to unphosphorylated ΔN-EphB6 in analytical SEC (Figure 4D), thus excluding a role for JM phosphorylation in EphB6 oligomerisation.

pJX2 is the major binding site for SH2 domain-containing signalling/adaptor proteins

Having established that EphB6 can be phosphorylated by EphB4, we next sought to understand if phosphorylated EphB6 can interact with SH2 domains. We selected the SH2 domains from the Abl, Vav2, Vav3, Nck1, Nck2, CrkII, CrkL, Grb7 and Grb10 signalling/adaptor proteins based on their consensus recognition sequence corresponding to that of the EphB6 phosphorylated tyrosine motif (Table 1). The majority of these SH2 domain-containing proteins was also reported to interact with other kinase-active Eph receptors [21]. We measured their binding affinities by SPR by immobilising the non-phosphorylated, low- (P$_L$) and high-degree (P$_H$) phosphorylated EphB6 isolated from anion exchange chromatography (Figure 4B) on the SPR chips as ligands, and used purified SH2 domains as the analytes. As expected, the SH2 domains did not bind to non-phosphorylated EphB6, whereas they displayed robust binding to both the P$_L$- and P$_H$-EphB6, with K_D values ranging 20–90 μM (Figure 5 and Supplementary Figure S5, and Table 1). SH2 domains generally display a low micromolar affinity for their tyrosine-phosphorylated binding partners [68], although it is important to note that the SH2 domain adaptors examined here typically co-occur with other protein interaction domains, such as SH3 domains, which together could enhance overall binding affinity through avidity effects.

To precisely pinpoint which of the four phosphorylated tyrosine residues on the JM region is critical for SH2 domain binding, we measured the binding affinities of the EphB6 JM peptides containing each of these individual phosphorylation sites. While we did not observe substantive binding to the EphB6 pY669 site, we found that a pJX2 (pY651)-containing peptide bound the Abl, Src and Vav3 SH2 domains with an affinity

Table 1. Binding affinities of SH2 domains against dephospho- and phospho-ΔN-EphB6

| Proteins tested	K_D of ΔN-EphB6	K_D of P_L-ΔN-EphB6	K_D of P_H-ΔN-EphB6	pY recognition sequence [65–67]	Full length-protein functions
Abl-SH2	Non-specific binding	45.4 ± 1.3	39.9 ± 1.8	Y-E/A-N(E)-P/V/L	Tyrosine kinase
Vav2-SH2*		19.3 ± 1.8	17.4 ± 2.0	Y-L-X-P	Guanine Exchange Factors (GEFs)
Vav3-SH2		32.2 ± 1.3	25.6 ± 1.0	No data, but high SH2 domain sequence similarity with Vav2-SH2	
Nck1-SH2		96.7 ± 6.5	69.0 ± 4.9	Y-D/E-X-V/P	Adaptor proteins
Nck2-SH2		70.2 ± 6.6	52.0 ± 4.0	Y-D/E-X-V/P	
CrkII-SH2		42.3 ± 3.4	30.0 ± 1.5	Y-X-X-P Or Y-D-L/V-P	
CrkL-SH2		49.9 ± 1.6	44.3 ± 1.2	Y-X-X-P Or Y-D-L/V-P	
Grb7-SH2*		26.0 ± 0.8	16.8 ± 0.5	P-Q-P-E-Y-N-Q-P-D	
Grb10-SH2*		26.1 ± 0.9	16.6 ± 0.4	No data, but high SH2 domain sequence similarity with Grb7-SH2	

Binding affinities, K_D in μM, were calculated by averaging three independent measurements. Errors represent the standard error of the mean (SEM). *Indicates proteins exist as dimers in solution.

equivalent to, or stronger than to those measured from the purified phosphorylated EphB6 (Figure 6 and Supplementary Figure S6; Tables 1 and 2). We observed a range of K_D values from 3 to 25 μM for EphB6 pJX2 binding to the Abl, Src and Vav3 SH2 domains, suggesting there is a hierarchy of affinities for downstream interactors, and some intrinsic selectivity (Table 2). Interestingly, the pJX1 (pY645) EphB6 peptide exhibited ~5-fold weaker binding affinity for Abl, Src and Vav3 SH2 domains compared with pJX2, indicating that pJX2 is the principal site for SH2 domain binding. Surprisingly, a synergistic effect was observed when Y644, JX1 and JX2 tyrosine residues were all phosphorylated. This triply phosphorylated EphB6 peptide bound all the SH2 domains tested with a low micromolar K_D (1–5 μM) (Figure 6C, Supplementary Figures S6C,I, and Table 2), which is a range of affinity typical of functional SH2 domain:phosphopeptide interactions in cells [68]. A previous study on EphA3 showed that the phosphorylation on its JM region occurs via sequential events, in which the JX2 tyrosine is first phosphorylated, followed by the JX1 tyrosine residue [62]. Our data suggest a similar hierarchy within the EphB6 JM domain might be possible, owing to a greater affinity of SH2 domains from Abl, Src and Vav3 for the EphB6 phosphoryated JX2 tyrosine residue, although this relative selectivity (at least with respect to Abl, Src and Vav3) is reduced when Y644, JX1 and JX2 tyrosine residues are all phosphorylated (Table 2). These data indicate that phosphorylation of the JX2 tyrosine confers a primary layer of selectivity for SH2 binding toward EphB6, while phosphorylation of the JX1 (Y645) and its adjacent tyrosine (Y644) may further enhance SH2 affinity but do so with reduced selectivity, enabling interaction with a broader repertoire of SH2-domain-containing proteins. This suggests differential phosphorylation within the JM region of EphB6 can drive diverse signalling output (Figure 7).

Discussion

Much of our understanding about the cellular roles of Eph receptors has been dominated by the catalytic activities of the kinase-active family members. However, the existence of the catalytically dead EphB6 and EphA10 receptor pseudokinases illustrates that the mechanistic details of Eph regulation are far from being completely resolved. While the lack of kinase activity in the EphB6 and EphA10 receptors has led to limited attention to their cellular roles, it is evident from the down-regulation of EphB6 expression in metastatic tumor tissue, and EphA10 overexpression in oncogenesis, that these proteins serve important signalling functions.

Here, we sought to address how the intracellular regions of the catalytically dead Eph receptor family members, EphB6 and EphA10, are organised and how they engage downstream signalling adaptors and effectors. Remarkably, not only the central pseudokinase domain, but also the flanking JM region and SAM domain
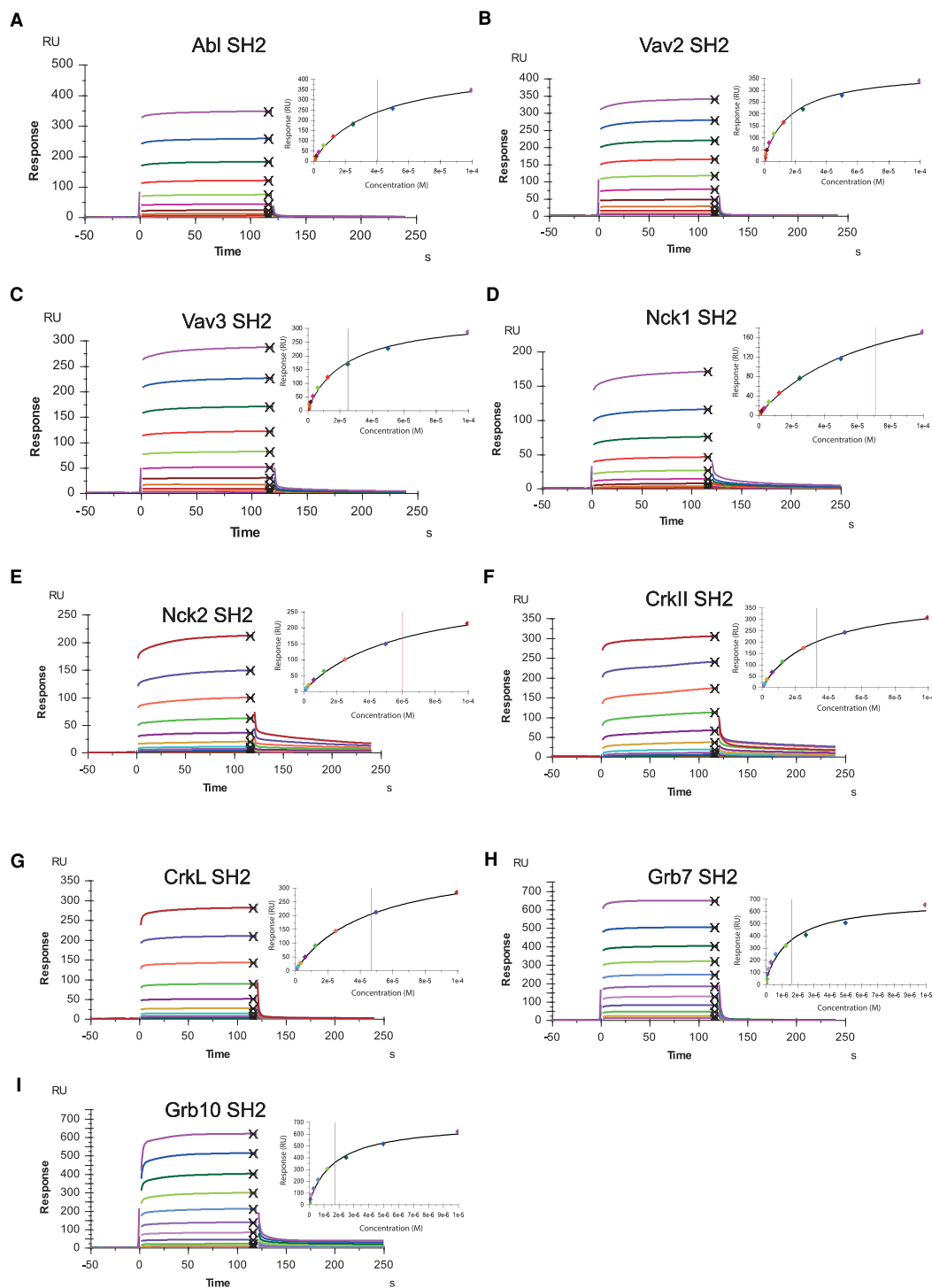
Figure 5. Binding of SH2 domains to the phosphorylated EphB6 (P$_H$-ΔN-EphB6) measured by surface plasmon resonance (SPR).

Binding of P$_H$-ΔN-EphB6 to the SH2 domains of Abl (**A**), Vav2 (**B**), Vav3 (**C**), Nck1 (**D**), Nck2 (**E**), CrkII (**F**), CrkL (**G**), Grb7 (**H**) and Grb10 (**I**). The immobilisation level of P$_H$-ΔN-EphB6 on the SA sensor chip was 1705.1 RU.

exhibit tremendous dynamicity. The central pseudokinase domains of both EphB6 and EphA10 lack catalytic activity, but our finding that each can bind ATP, Type I and Type II kinase inhibitors suggests these domains are dynamic and their conformations could be modulated by small-molecule binders. The precise effect such
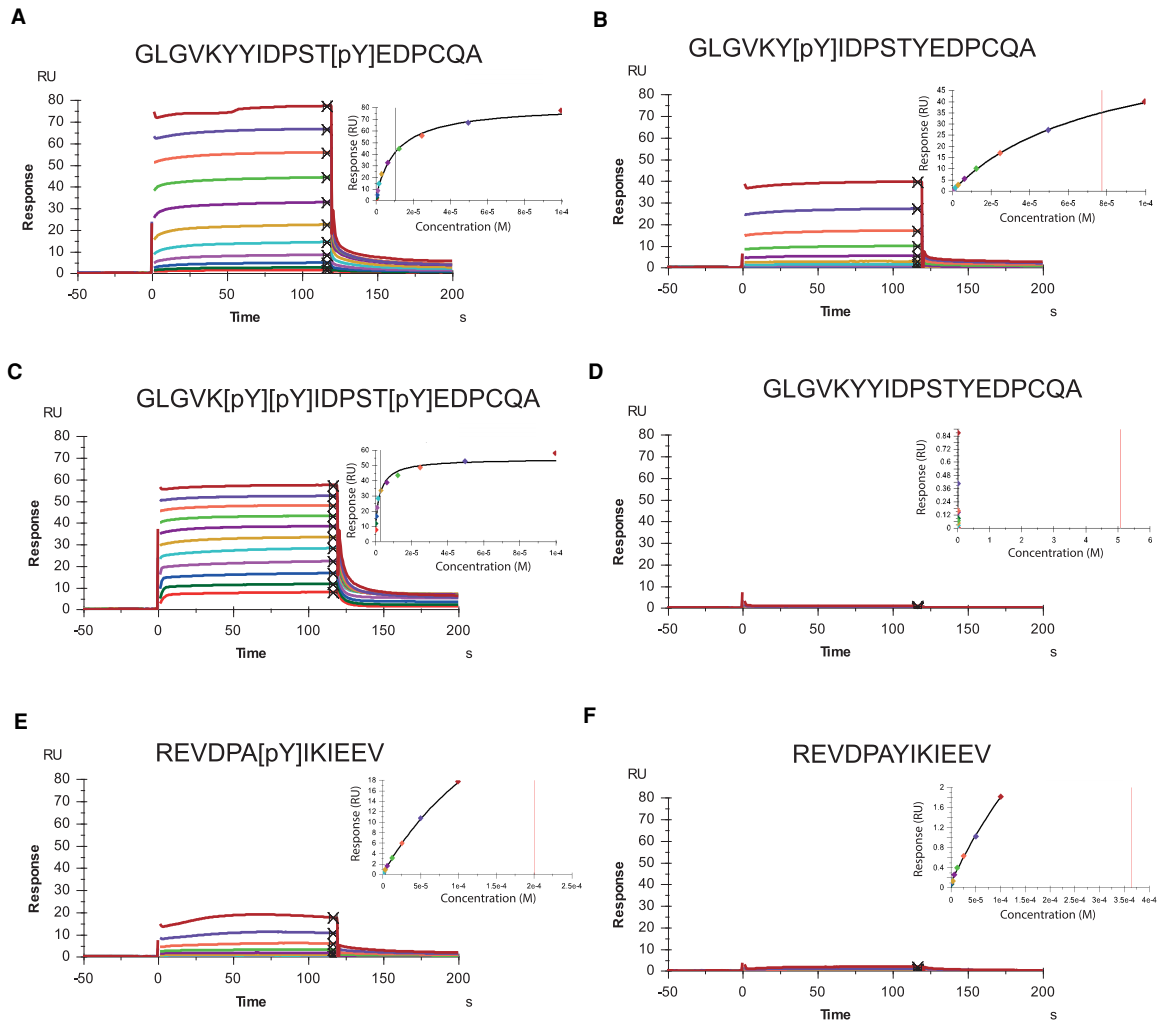
Figure 6. Binding of Abl SH2 domain to different phosphorylated EphB6 peptides measured by surface plasmon resonance (SPR).

Binding of Abl SH2 domain to pJX2 EphB6 peptide (**A**), pJX1 EphB6 peptide (**B**) and p644, pJX1 and pJX2 tri-phospho EphB6 peptide (**C**). (**D**) No binding was observed for the non-phosphorylated EphB6 peptide and Abl SH2 domain. (**E**) p669 EphB6 peptide binding to Abl SH2 domain. (**F**) No binding was observed for the non-phosphorylated EphB6 peptide and Abl SH2 domain. The immobilisation level of Abl SH2 domain on the CM5 chip was 1599.5 RU.

conformational modulation would have on the domains flanking the pseudokinase domain in EphB6 and EphA10 remains an open question. It is possible that conformational changes in the pseudokinase domain could impact its capacity to engage the SAM domain *in cis*, which would enable the N-terminal segment of the SAM domain α5 helix to be more readily available for SAM–SAM interactions, like those reported for other Eph receptors [52]. Similarly, EphB6 and EphA10 pseudokinase domain conformational modulation may lead to greater access of the JM region to downstream effector proteins and, in the case of EphB6, allowing phosphorylation by EphB4.

The phosphorylation catalysed by kinase-competent Eph receptors is an essential element of their capacity to propagate cytoplasmic signals. Ephrin ligation to the Eph receptor ectodomains promotes receptor oligomerisation, which in turn amplifies Eph receptor autophosphorylation as an upstream signalling event. The conserved JX1 and JX2 tyrosines located on the C-terminal portion of the JM region are the key phosphorylation sites that govern Eph receptor kinase activity and interaction with SH2 domain-containing effectors. While previous studies using overexpressed receptors have implicated EphB6 as an EphB4 substrate [30], here we have

**Table 2. Binding affinities of EphB6 peptides against SH2 domains**

Proteins/peptides tested	Abl-SH2	Src-SH2	Vav3-SH2
GLGVKYYIDPSTYEDPCQA	N.D.	N.D.	N.D.
GLGVKYYIDPST**[pY]**EDPCQA (pY651 = pJX2)	11.2 ± 0.8	24.6 ± 3.0	3.4 ± 0.6
GLGVKY**[pY]**IDPSTYEDPCQA (pY645 = pJX1)	72.5 ± 2.8	>100	27.9 ± 2.7
GLGVK**[pY][pY]**IDPST**[pY]**EDPCQA (pY644, pY645 (JX1) and pY651 (JX2))	2.3 ± 0.4	4.9 ± 0.4	1.1 ± 0.1
REVDPAYIKIEEV	N.D.	N.D.	N.D.
REVDPA**[pY]**IKIEEV (pY669)	>100	>100	>100

Binding affinities, K_D, in µM, were calculated by averaging three independent measurements. Errors represent the standard error of the mean (SEM).

pinpointed the substrate residues using biochemical approached and mass spectrometry. Our finding that EphB4 phosphorylates the EphB6 JM region raises the prospect that other Eph receptors could similarly phosphorylate others *in trans* to induce their recruitment of SH2 domain-containing signalling adaptors and effectors (Figure 7). In contrast with EphB6 and other Eph receptor family members, EphA10 lacks the JX1 and JX2 tyrosine residues in its JM region through substitution with phenylalanine and cysteine, respectively. The JX1 substitution of tyrosine for phenylalanine is structurally conservative, but precludes phosphorylation and interaction with SH2 domain-containing effectors, while it is possible that the JX2 cysteine may act as a redox sensor, a regulatory mechanism adopted by other protein kinases [70,71]. The expression of EphA10 in normal tissues is restricted to the testes, but elevated in multiple types of cancer. Because of the hypoxia and free oxygen radicals that is experienced by tumour cells, it is possible that up-regulation of EphA10 could play a role in sensing oxidative stress and that oxidation of the JX2 cysteine could influence interactions with downstream effectors and ensuing signal transduction. The identities of the downstream effectors of EphA10 and how they are engaged in the absence of the conventional JX1 and JX2 phosphotyrosines remains of outstanding interest.

Evolutionarily, the amino acid sequences of the human Eph receptors share greater than 90% identity with their mouse orthologues, including EphB6 and EphA10, which similarly lack key catalytic residues and are also pseudokinases in rodents. Interestingly, only EphB6 orthologues in mammals are predicted to be catalytically inactive, while those in fish, reptiles and birds are predicted to be catalytically active owing to the retention of all the essential catalytic residues to catalyse ATP hydrolysis. In contrast with the truncated activation loop in the human EphB6, the zebrafish orthologue has an intact loop containing a conserved tyrosine residue, suggesting a role in activating kinase once phosphorylated. Although it requires experimental validation, all these characteristics suggest that the zebrafish EphB6 is a catalytically active kinase and that the ancestral form of the protein, which likely arose through duplication of an Eph receptor gene, is likely to be an active kinase. The conserved tyrosines on the JM region in human EphB6, and their ability to bind SH2 domains once phosphorylated, have likely manifested the signalling properties inherited from their ancestral kinase-active form. Unlike EphB6, all EphA10 orthologues lack the essential catalytic residues and are thus categorised as pseudokinases. While a tyrosine residue in the JX1 position is present in some orthologues, including the Japanese rice fish, all known EphA10 orthologues possess a cysteine residue at the JX2 position. The conservation of a cysteine residue on this salient position throughout species may imply an irreplaceable role of EphA10 pseudokinase in redox sensing and signal transduction, although the precise role of the JX2 cysteine in EphA10 regulation awaits further investigation. Meanwhile, whether the repertoire of interaction partners bound by the EphB6 JX2 pTyr is common between orthologues, remains an open question for future investigation.

Together, our data suggest the EphB6 and EphA10 pseudokinase domains may serve several functions in cells: as a hub for the assembly of signalling complexes, as for example, observed for the PEAK pseudokinases SgK223 and SgK269 [57,72]; as a possible conformational switch, as proposed for other pseudokinases, such as MLKL [9,50]; and possibly as an allosteric regulator of catalytically active Eph receptors, as observed for HER3 regulation of EGFR [7]. Additionally, while most studies of catalytically active Eph receptors to date have
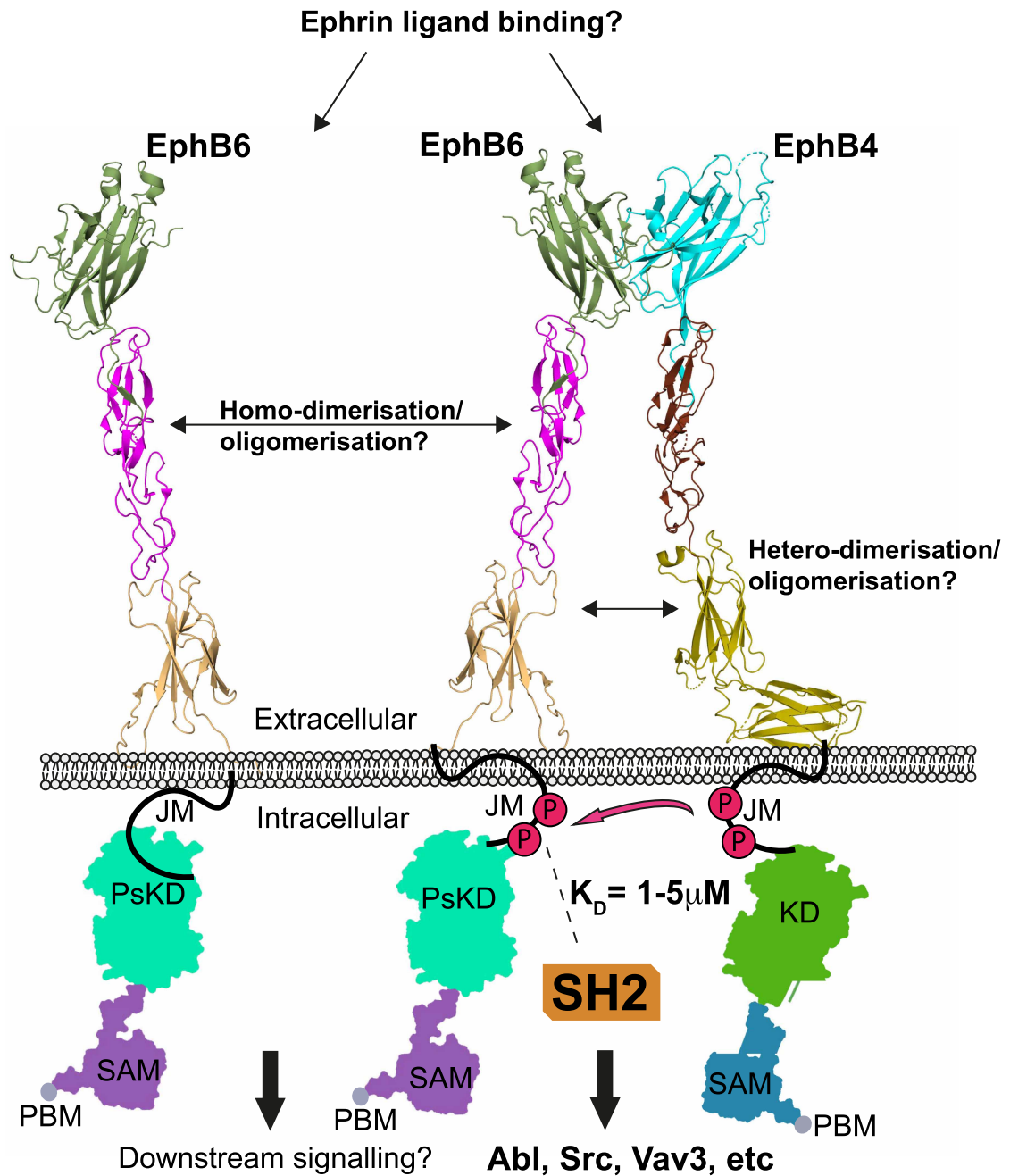
Figure 7. Proposed model for signalling by the EphB6 pseudokinase.

The ectodomains of EphB6 and EphB4 can potentially dimerise and oligomerise following the binding of ephrin ligands. Upon dimerisation, the EphB4 kinase domain undergoes autophosphorylation, and then phosphorylates the JM region of EphB6. The phosphorylated EphB6 JM region can then serve as a docking site for downstream SH2 domain-containing signalling adaptors, such as Src, Abl and Vav3. Therefore, phosphorylated EphB6 can promote the assembly of specific signalling hub depending on the SH2 domain-containing proteins recruited. However, whether EphB6 can also potentially homodimerise/ oligomerise upon binding to ephrin ligands and amplify the recruitment of downstream interactors to elicit EphB6 specific driven signalling output remains to be investigated. The crystal structure of the EphB6 ectodomains (PDB: 7K7J [69]) was used to generate the schematic illustration of the EphB6 ectodomains. The crystal structure of the EphA2 ectodomains (PDB: 3FL7 [51]) was used to generate the schematic illustration of the EphB4 ectodomains. SH2: SH2 domain-containing proteins. JM: juxtamembrane region. PsKD: pseudokinase domain. KD: kinase domain. SAM: sterile-α-motif domain. PBM: PDZ domain-binding motif.

focused on the roles of their kinase activity, our findings support a crucial role for their non-catalytic functions in mediating signal transduction. The dynamics of engagement of downstream effectors, and their cellular contexts, remain of enormous interest to understanding both kinase-competent and pseudokinase Eph receptors.

Data Availability

All data and reagents are available from the authors upon request.

Competing Interests

The authors declare that there are no competing interests associated with the manuscript.

CRediT Author Contribution

Lung-Yu Liang: Conceptualization, formal analysis, investigation, methodology, writing — original draft. **Michael Roy**: Investigation, methodology, supervision, writing — review and editing. **Christopher R. Horne**: Investigation, methodology. **Jarrod J. Sandow**: Investigation. **Minglyanna Surudoi**: Methodology. **Laura F. Dagley**: Investigation, methodology. **Samuel N. Young**: Methodology. **Toby Dite**: Formal analysis, methodology. **Jeffrey J. Babon**: Investigation, writing — review and editing. **Peter W. Janes**: Conceptualization, investigation, writing — review and editing. **Onisha Patel**: Conceptualization, supervision, methodology, writing — review and editing. **James M. Murphy**: Conceptualization, supervision, funding acquisition, writing — review and editing. **Isabelle S. Lucet**: Conceptualization, supervision, funding acquisition, writing — review and editing.

Abbreviations

FDR, false discovery rate; JM, juxtamembrane; PBM, PDZ domain-binding motif; RTKs, receptor tyrosine kinases; SAXS, small-angle X-ray scattering; SBP, streptavidin binding peptide; SPR, surface plasmon resonance.

References

1 Lemmon, M.A. and Schlessinger, J. (2010) Cell signaling by receptor tyrosine kinases. *Cell* **141**, 1117–1134 https://doi.org/10.1016/j.cell.2010.06.011

2 Mendrola, J.M., Shi, F., Park, J.H. and Lemmon, M.A. (2013) Receptor tyrosine kinases with intracellular pseudokinase domains. *Biochem. Soc. Trans.* **41**, 1029–1036 https://doi.org/10.1042/BST20130104

3 Jacobsen, A.V. and Murphy, J.M. (2017) The secret life of kinases: insights into non-catalytic signalling functions from pseudokinases. *Biochem. Soc. Trans.* **45**, 665–681 https://doi.org/10.1042/BST20160331

4 Reiterer, V., Eyers, P.A. and Farhan, H. (2014) Day of the dead: pseudokinases and pseudophosphatases in physiology and disease. *Trends Cell Biol.* **24**, 489–505 https://doi.org/10.1016/j.tcb.2014.03.008

5 Lucet, I.S. and Murphy, J.M. (2019) CHAPTER 13 A structural perspective of the pseudokinome: defining the targetable space. In *Kinase Drug Discovery: Modern Approaches*, pp. 359–380, The Royal Society of Chemistry, London, UK

6 Mace, P.D. and Murphy, J.M. (2021) There's more to death than life: non-catalytic functions in kinase and pseudokinase signaling. *J. Biol. Chem.* **296**, 100705 https://doi.org/10.1016/j.jbc.2021.100705

7 Littlefield, P., Liu, L., Mysore, V., Shan, Y., Shaw, D.E. and Jura, N. (2014) Structural analysis of the EGFR/HER3 heterodimer reveals the molecular basis for activating HER3 mutations. *Sci. Signal.* **7**, ra114 https://doi.org/10.1126/scisignal.2005786

8 Patel, O., Roy, M.J., Murphy, J.M. and Lucet, I.S. (2020) The PEAK family of pseudokinases, their role in cell signalling and cancer. *FEBS J.* **287**, 4183–4197 https://doi.org/10.1111/febs.15087

9 Garnish, S.E., Meng, Y., Koide, A., Sandow, J.J., Denbaum, E., Jacobsen, A.V. et al. (2021) Conformational interconversion of MLKL and disengagement from RIPK3 precede cell death by necroptosis. *Nat. Commun.* **12**, 2211 https://doi.org/10.1038/s41467-021-22400-z

10 Murphy, J.M., Czabotar, P.E., Hildebrand, J.M., Lucet, I.S., Zhang, J.G., Alvarez-Diaz, S. et al. (2013) The pseudokinase MLKL mediates necroptosis via a molecular switch mechanism. *Immunity* **39**, 443–453 https://doi.org/10.1016/j.immuni.2013.06.018

11 Petrie, E.J., Sandow, J.J., Lehmann, W.I.L., Liang, L.Y., Coursier, D., Young, S.N. et al. (2019) Viral MLKL homologs subvert necroptotic cell death by sequestering cellular RIPK3. *Cell Rep.* **28**, 3309–3319.e3305 https://doi.org/10.1016/j.celrep.2019.08.055

12 Sheetz, J.B., Mathea, S., Karvonen, H., Malhotra, K., Chatterjee, D., Niininen, W. et al. (2020) Structural insights into pseudokinase domains of receptor tyrosine kinases. *Mol. Cell* **79**, 390–405.e397 https://doi.org/10.1016/j.molcel.2020.06.018

13 Artim, S.C., Mendrola, J.M. and Lemmon, M.A. (2012) Assessing the range of kinase autoinhibition mechanisms in the insulin receptor family. *Biochem. J.* **448**, 213–220 https://doi.org/10.1042/BJ20121365

14 Kung, J.E. and Jura, N. (2019) Prospects for pharmacological targeting of pseudokinases. *Nat. Rev. Drug Discov.* **18**, 501–526 https://doi.org/10.1038/s41573-019-0018-3

15 Lang, B., Pu, J., Hunter, I., Liu, M., Martin-Granados, C., Reilly, T.J. et al. (2014) Recurrent deletions of ULK4 in schizophrenia: a gene crucial for neuritogenesis and neuronal motility. *J. Cell Sci.* **127**, 630–640 https://doi.org/10.1242/jcs.137604

16 Zhou, H., Yu, M., Fukuda, K., Im, J., Yao, P., Cui, W. et al. (2013) IRAK-M mediates Toll-like receptor/IL-1R-induced NFkappaB activation and cytokine production. *EMBO J.* **32**, 583–596 https://doi.org/10.1038/emboj.2013.2

17 Wilkinson, D.G. (2014) Regulation of cell differentiation by Eph receptor and ephrin signaling. *Cell Adh. Migr.* **8**, 339–348 https://doi.org/10.4161/19336918.2014.970007

18 Lisabeth, E.M., Falivelli, G. and Pasquale, E.B. (2013) Eph receptor signaling and ephrins. *Cold Spring Harb. Perspect. Biol.* **5**, a009159 https://doi.org/10.1101/cshperspect.a009159

19 Nievergall, E., Lackmann, M. and Janes, P.W. (2012) Eph-dependent cell-cell adhesion and segregation in development and cancer. *Cell Mol. Life Sci.* **69**, 1813–1842 https://doi.org/10.1007/s00018-011-0900-6

20 Pasquale, E.B. (2010) Eph receptors and ephrins in cancer: bidirectional signalling and beyond. *Nat. Rev. Cancer* **10**, 165–180 https://doi.org/10.1038/nrc2806

21 Liang, L.Y., Patel, O., Janes, P.W., Murphy, J.M. and Lucet, I.S. (2019) Eph receptor signalling: from catalytic to non-catalytic functions. *Oncogene* **38**, 6567–6584 https://doi.org/10.1038/s41388-019-0931-2

22 Peng, L., Tu, P., Wang, X., Shi, S., Zhou, X. and Wang, J. (2014) Loss of EphB6 protein expression in human colorectal cancer correlates with poor prognosis. *J. Mol. Histol.* **45**, 555–563 https://doi.org/10.1007/s10735-014-9577-0

23 Mateo-Lozano, S., Bazzocco, S., Rodrigues, P., Mazzolini, R., Andretta, E., Dopeso, H. et al. (2017) Loss of the EPH receptor B6 contributes to colorectal cancer metastasis. *Sci. Rep.* **7**, 43702 https://doi.org/10.1038/srep43702

24 Yu, J., Bulk, E., Ji, P., Hascher, A., Tang, M., Metzger, R. et al. (2010) The EPHB6 receptor tyrosine kinase is a metastasis suppressor that is frequently silenced by promoter DNA hypermethylation in non-small cell lung cancer. *Clin. Cancer Res.* **16**, 2275–2283 https://doi.org/10.1158/1078-0432.CCR-09-2000

25 Nagano, K., Kanasaki, S.-I., Yamashita, T., Maeda, Y., Inoue, M., Higashisaka, K. et al. (2013) Expression of Eph receptor A10 is correlated with lymph node metastasis and stage progression in breast cancer patients. *Cancer Med.* **2**, 972–977 https://doi.org/10.1002/cam4.156

26 Toosi, B.M., El Zawily, A., Truitt, L., Shannon, M., Allonby, O., Babu, M. et al. (2018) EPHB6 augments both development and drug sensitivity of triple-negative breast cancer tumours. *Oncogene* **37**, 4073–4093 https://doi.org/10.1038/s41388-018-0228-x

27 Nagano, K., Yamashita, T., Inoue, M., Higashisaka, K., Yoshioka, Y., Abe, Y. et al. (2014) Eph receptor A10 has a potential as a target for a prostate cancer therapy. *Biochem. Biophys. Res. Commun.* **450**, 545–549 https://doi.org/10.1016/j.bbrc.2014.06.007

28 Akada, M., Harada, K., Negishi, M. and Katoh, H. (2014) Ephb6 promotes anoikis by modulating EphA2 signaling. *Cell Signal.* **26**, 2879–2884 https://doi.org/10.1016/j.cellsig.2014.08.031

29 Freywald, A., Sharfe, N. and Roifman, C.M. (2002) The kinase-null EphB6 receptor undergoes transphosphorylation in a complex with EphB1. *J. Biol. Chem.* **277**, 3823–3828 https://doi.org/10.1074/jbc.M108011200

30 Truitt, L., Freywald, T., DeCoteau, J., Sharfe, N. and Freywald, A. (2010) The EphB6 receptor cooperates with c-Cbl to regulate the behavior of breast cancer cells. *Cancer Res.* **70**, 1141–1153 https://doi.org/10.1158/0008-5472.CAN-09-1710

31 Matsuoka, H., Obama, H., Kelly, M.L., Matsui, T. and Nakamoto, M. (2005) Biphasic functions of the kinase-defective Ephb6 receptor in cell adhesion and migration. *J. Biol. Chem.* **280**, 29355–29363 https://doi.org/10.1074/jbc.M500010200

32 Murphy, J.M., Zhang, Q., Young, S.N., Reese, M.L., Bailey, F.P., Eyers, P.A. et al. (2014) A robust methodology to subclassify pseudokinases based on their nucleotide-binding properties. *Biochem. J.* **457**, 323–334 https://doi.org/10.1042/BJ20131174

33 Oliver, M.R., Horne, C.R., Shrestha, S., Keown, J.R., Liang, L.Y., Young, S.N. et al. (2021) Granulovirus PK-1 kinase activity relies on a side-to-side dimerization mode centered on the regulatory alphaC helix. *Nat. Commun.* **12**, 1002 https://doi.org/10.1038/s41467-021-21191-7

34 Davies, K.A., Fitzgibbon, C., Young, S.N., Garnish, S.E., Yeung, W., Coursier, D. et al. (2020) Distinct pseudokinase domain conformations underlie divergent activation mechanisms among vertebrate MLKL orthologues. *Nat. Commun.* **11**, 3060 https://doi.org/10.1038/s41467-020-16823-3

35 Schiffrin, B., Radford, S.E., Brockwell, D.J. and Calabrese, A.N. (2020) Pyxlinkviewer: a flexible tool for visualization of protein chemical crosslinking data within the PyMOL molecular graphics system. *Protein Sci.* **29**, 1851–1857 https://doi.org/10.1002/pro.3902

36 Kirby, N., Cowieson, N., Hawley, A.M., Mudie, S.T., McGillivray, D.J., Kusel, M. et al. (2016) Improved radiation dose efficiency in solution SAXS using a sheath flow sample environment. *Acta Crystallogr. D Struct. Biol.* **72**, 1254–1266 https://doi.org/10.1107/S2059798316017174

37 Ryan, T.M., Trewhella, J., Murphy, J.M., Keown, J.R., Casey, L., Pearce, F.G. et al. (2018) An optimized SEC-SAXS system enabling high X-ray dose for rapid SAXS assessment with correlated UV measurements for biomolecular structure analysis. *J. Appl. Crystallogr.* **51**, 97–111 https://doi.org/10.1107/S1600576717017101

38 Manalastas-Cantos, K., Konarev, P.V., Hajizadeh, N.R., Kikhney, A.G., Petoukhov, M.V., Molodenskiy, D.S. et al. (2021) ATSAS 3.0: expanded functionality and new tools for small-angle scattering data analysis. *J. Appl. Crystallogr.* **54**, 343–355 https://doi.org/10.1107/S1600576720013412

39 Piiadov, V., Ares de Araujo, E., Oliveira Neto, M., Craievich, A.F. and Polikarpov, I. (2019) SAXSMow 2.0: online calculator of the molecular weight of proteins in dilute solution from experimental SAXS data measured on a relative scale. *Protein Sci.* **28**, 454–463 https://doi.org/10.1002/pro.3528

40 Svergun, D.I., Barberato, C. and Koch, M.H.J. (1995) CRYSOL - a program to evaluate X-ray solution scattering of biological macromolecules from atomic coordinates. *J. Appl. Cryst.* **28**, 768–773 https://doi.org/10.1107/S0021889895007047

41 Lechtenberg, B.C., Gehring, M.P., Light, T.P., Matsumoto, M.W., Hristova, K. and Pasquale, E.B. (2021) Allosteric regulation of the EphA2 receptor intracellular region by serine/threonine kinases. *BioRxiv* https://doi.org/10.1101/2021.01.28.428700

42 Jumper, J., Evans, R., Pritzel, A., Green, T., Figurnov, M., Ronneberger, O. et al. (2021) Highly accurate protein structure prediction with AlphaFold. *Nature* **596**, 583–589 https://doi.org/10.1038/s41586-021-03819-2

43 Wisniewski, J.R., Zougman, A., Nagaraj, N. and Mann, M. (2009) Universal sample preparation method for proteome analysis. *Nat. Methods* **6**, 359–362 https://doi.org/10.1038/nmeth.1322

44 Delconte, R.B., Kolesnik, T.B., Dagley, L.F., Rautela, J., Shi, W., Putz, E.M. et al. (2016) CIS is a potent checkpoint in NK cell-mediated tumor immunity. *Nat. Immunol.* **17**, 816–824 https://doi.org/10.1038/ni.3470

45 Cox, J., Neuhauser, N., Michalski, A., Scheltema, R.A., Olsen, J.V. and Mann, M. (2011) Andromeda: a peptide search engine integrated into the MaxQuant environment. *J. Proteome Res.* **10**, 1794–1805 https://doi.org/10.1021/pr101065j

46 Brademan, D.R., Riley, N.M., Kwiecien, N.W. and Coon, J.J. (2019) Interactive peptide spectral annotator: a versatile web-based tool for proteomic applications. *Mol. Cell. Proteom.* **18**, S193–S201 https://doi.org/10.1074/mcp.TIR118.001209

47 Wybenga-Groot, L.E., Baskin, B., Ong, S.H., Tong, J., Pawson, T. and Sicheri, F. (2001) Structural basis for autoinhibition of the Ephb2 receptor tyrosine kinase by the unphosphorylated juxtamembrane region. *Cell* **106**, 745–757 https://doi.org/10.1016/S0092-8674(01)00496-2

48 Davis, T.L., Walker, J.R., Loppnau, P., Butler-Cole, C., Allali-Hassani, A. and Dhe-Paganon, S. (2008) Autoregulation by the Juxtamembrane region of the human ephrin receptor tyrosine kinase A3 (EphA3). *Structure* **16**, 873–884 https://doi.org/10.1016/j.str.2008.03.008

49 Knight, Z.A. and Shokat, K.M. (2005) Features of selective kinase inhibitors. *Chem. Biol.* **12**, 621–637 https://doi.org/10.1016/j.chembiol.2005.04.011

50 Petrie, E.J., Sandow, J.J., Jacobsen, A.V., Smith, B.J., Griffin, M.D.W., Lucet, I.S. et al. (2018) Conformational switching of the pseudokinase domain promotes human MLKL tetramerization and cell death by necroptosis. *Nat. Commun.* **9**, 2422 https://doi.org/10.1038/s41467-018-04714-7

51 Himanen, J.P., Yermekbayeva, L., Janes, P.W., Walker, J.R., Xu, K., Atapattu, L. et al. (2010) Architecture of Eph receptor clusters. *Proc. Natl Acad. Sci. U.S.A.* **107**, 10860–10865 https://doi.org/10.1073/pnas.1004148107

52 Wang, Y., Shang, Y., Li, J., Chen, W., Li, G., Wan, J. et al. (2018) Specific Eph receptor-cytoplasmic effector signaling mediated by SAM–SAM domain interactions. *eLife* **7**, e35677 https://doi.org/10.7554/eLife.35677

53 Stapleton, D., Balan, I., Pawson, T. and Sicheri, F. (1999) The crystal structure of an Eph receptor SAM domain reveals a mechanism for modular dimerization. *Nat. Struct. Biol.* **6**, 44–49 https://doi.org/10.1038/4917

54 Thanos, C.D., Goodwill, K.E. and Bowie, J.U. (1999) Oligomeric structure of the human EphB2 receptor SAM domain. *Science* **283**, 833–836 https://doi.org/10.1126/science.283.5403.833

55 Singh, D.R., Cao, Q., King, C., Salotto, M., Ahmed, F., Zhou, X.Y. et al. (2015) Unliganded EphA3 dimerization promoted by the SAM domain. *Biochem. J.* **471**, 101–109 https://doi.org/10.1042/BJ20150433

56 Light, T.P., Gomez-Soler, M., Wang, Z., Karl, K., Zapata-Mercado, E., Gehring, M.P. et al. (2021) A cancer mutation promotes EphA4 oligomerization and signaling by altering the conformation of the SAM domain. *J. Biol. Chem.* **297**, 100876 https://doi.org/10.1016/j.jbc.2021.100876

57 Patel, O., Griffin, M.D.W., Panjikar, S., Dai, W., Ma, X., Chan, H. et al. (2017) Structure of SgK223 pseudokinase reveals novel mechanisms of homotypic and heterotypic association. *Nat. Commun.* **8**, 1157 https://doi.org/10.1038/s41467-017-01279-9

58 Zhang, X., Gureasko, J., Shen, K., Cole, P.A. and Kuriyan, J. (2006) An allosteric mechanism for activation of the kinase domain of epidermal growth factor receptor. *Cell* **125**, 1137–1149 https://doi.org/10.1016/j.cell.2006.05.013

59 Jura, N., Endres, N.F., Engel, K., Deindl, S., Das, R., Lamers, M.H. et al. (2009) Mechanism for activation of the EGF receptor catalytic domain by the juxtamembrane segment. *Cell* **137**, 1293–1307 https://doi.org/10.1016/j.cell.2009.04.025

60 Borthakur, S., Lee, H., Kim, S., Wang, B.C. and Buck, M. (2014) Binding and function of phosphotyrosines of the Ephrin A2 (EphA2) receptor using synthetic sterile alpha motif (SAM) domains. *J. Biol. Chem.* **289**, 19694–19703 https://doi.org/10.1074/jbc.M114.567602

61 Han, D.C., Shen, T.L., Miao, H., Wang, B. and Guan, J.L. (2002) Ephb1 associates with Grb7 and regulates cell migration. *J. Biol. Chem.* **277**, 45655–45661 https://doi.org/10.1074/jbc.M203165200

62 Kwon, A., John, M., Ruan, Z. and Kannan, N. (2018) Coupled regulation by the juxtamembrane and sterile alpha motif (SAM) linker is a hallmark of ephrin tyrosine kinase evolution. *J. Biol. Chem.* **293**, 5102–5116 https://doi.org/10.1074/jbc.RA117.001296

63 Wiesner, S., Wybenga-Groot, L.E., Warner, N., Lin, H., Pawson, T., Forman-Kay, J.D. et al. (2006) A change in conformational dynamics underlies the activation of Eph receptor tyrosine kinases. *EMBO J.* **25**, 4686–4696 https://doi.org/10.1038/sj.emboj.7601315

64 Begley, M.J., Yun, C.H., Gewinner, C.A., Asara, J.M., Johnson, J.L., Coyle, A.J. et al. (2015) EGF-receptor specificity for phosphotyrosine-primed substrates provides signal integration with Src. *Nat. Struct. Mol. Biol.* **22**, 983–990 https://doi.org/10.1038/nsmb.3117

65 Tinti, M., Kiemer, L., Costa, S., Miller, M.L., Sacco, F., Olsen, J.V. et al. (2013) The SH2 domain interaction landscape. *Cell Rep.* **3**, 1293–1305 https://doi.org/10.1016/j.celrep.2013.03.001

66 Liu, B.A., Jablonowski, K., Shah, E.E., Engelmann, B.W., Jones, R.B. and Nash, P.D. (2010) SH2 domains recognize contextual peptide sequence information to determine selectivity. *Mol. Cell. Proteom.* **9**, 2391–2404 https://doi.org/10.1074/mcp.M110.001586

67 Janes, P.W., Lackmann, M., Church, W.B., Sanderson, G.M., Sutherland, R.L. and Daly, R.J. (1997) Structural determinants of the interaction between the erbB2 receptor and the Src homology 2 domain of Grb7. *J. Biol. Chem.* **272**, 8490–8497 https://doi.org/10.1074/jbc.272.13.8490

68 Kaneko, T., Joshi, R., Feller, S.M. and Li, S.S. (2012) Phosphotyrosine recognition domains: the typical, the atypical and the versatile. *Cell Commun. Signal.* **10**, 32 https://doi.org/10.1186/1478-811X-10-32

69 Mason, E.O., Goldgur, Y., Robev, D., Freywald, A., Nikolov, D.B. and Himanen, J.P. (2021) Structure of the EphB6 receptor ectodomain. *PLoS One* **16**, e0247335 https://doi.org/10.1371/journal.pone.0247335

70 Heppner, D.E., Dustin, C.M., Liao, C., Hristova, M., Veith, C., Little, A.C. et al. (2018) Direct cysteine sulfenylation drives activation of the Src kinase. *Nat. Commun.* **9**, 4522 https://doi.org/10.1038/s41467-018-06790-1

71 Byrne, D.P., Shrestha, S., Galler, M., Cao, M., Daly, L.A., Campbell, A.E. et al. (2020) Aurora A regulation by reversible cysteine oxidation reveals evolutionarily conserved redox control of Ser/Thr protein kinase activity. *Sci. Signal.* **13**, eaax2713 https://doi.org/10.1126/scisignal.aax2713

72 Liu, L., Phua, Y.W., Lee, R.S., Ma, X., Jenkins, Y., Novy, K. et al. (2016) Homo- and heterotypic association regulates signaling by the SgK269/PEAK1 and SgK223 pseudokinases. *J. Biol. Chem.* **291**, 21571–21583 https://doi.org/10.1074/jbc.M116.748897